

BIOMASS RESOURCES TO SUPPORT A LOW CARBON FUTURE

Ralph P. Overend

National Renewable Energy Laboratory
1617 Cole Boulevard, Golden, Colorado, USA

Introduction

The growing acceptance of biomass as the only renewable source of carbon for the future requires that a realistic appraisal of its potential be undertaken. While solar energy captured by wind, PV or high temperature concentrating solar systems, have very high energy supply potentials—far exceeding today's total primary energy supply of approximately 417 EJ (IEA, TPES data for 2000)—it will be delivered in the form of electricity and potentially hydrogen. However, before a purely hydrogen and electrical economy can arrive, during the 21st century the world has to undergo a carbon usage transition from directly emitting fossil carbon dioxide into the atmosphere to one in which fossil carbon is captured and sequestered, and biomass becomes the sole form of the earth's carbon resource that can be emitted directly to the atmosphere due to its short term photosynthetic cycle in the biosphere.

Unlike fossil fuels for which exploration, discovery and assessment of resources and reserves is a well known science, renewable energy accounting introduces a flow concept to describe the size and availability of the resource. Biomass is rather unusual; it exists somewhere between the intermittent, flux-only resources such as solar and wind, and the traditional fossil fuel stock perspective. This is because of its annual and perennial storage capability, allowing dispersed and captured solar energy to be concentrated and converted into useful, energy and products on a continuous basis at centralized facilities according to normal demand patterns. Thus, the photosynthesis process of solar collection, crop harvest, and transport of biomass fuels will define the availability of biomass for energy and materials purposes.

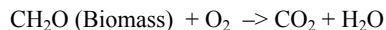
As with fossil resources, the energy conversion technologies play a huge role in enabling the solar resources by dictating the efficiency, and the utility of renewables with respect to society and the environment—in sum, their sustainability. However, this presentation will concentrate on the biomass system only up to the conversion plant gate.

Biomass resources in the USA

The renewable energy cycle for biomass starts with photosynthesis, which captures the fraction of light between 400 nm and 700 nm in the solar spectrum to provide the energy to fix carbon dioxide and split water molecules, producing raw photosynthate according to the equation:



The photosynthate formula, CH₂O, is essentially the same as sugar, starch, or cellulose, the latter being the most common natural polymer on earth. Energy is obtained from biomass by means of combustion with oxygen as in a fire, or through metabolic processes, e.g., respiration to provide chemical energy for muscles and other processes:



Either way, the net result is a closed cycle in which carbon dioxide and water vapor are returned to the atmosphere. This solar-energy powered closed-loop supports all life on earth, providing food for humanity, feed for animals, fibers for clothing, and materials for buildings and consumer products, in addition to fuel.

A theoretical estimate of the efficiency of photosynthesis is about 5.5%. The energy received from the sun at any given location varies with latitude and season; and the annual photosynthetic capture is a function of the water and nutrient availability and the seasonal climate variations. As a result actual crops achieve much less than this. The variation is very large ranging from the annual accumulation of less than 1 t ha⁻¹ y⁻¹ of dry biomass in a mature boreal forest, to approximately 50 t ha⁻¹ y⁻¹ of total biomass for a record corn yield (in Iowa, in 1999) of 408.2 bushels of corn per acre. This is calculated by accounting for the stalk and other above ground biomass components by means of the harvest index, which has a value of 0.5 applied to the 25.6 t ha⁻¹ y⁻¹ of corn kernels.

Sources of bioenergy

The primary biomass sources are natural forests, planted trees and shrubs, and agricultural crops. However, much of today's bioenergy is derived from secondary, tertiary, and post-consumer residues derived from these primary resources. Secondary residues are mainly harvesting residues and include: forest slash; crop residues such as straw and stover from cereal production; as well as minor sources such as orchard, rights of way, and vineyard prunings. Tertiary sources are usually process residues and include: black liquor produced in kraft pulping; sawdust and bark from solid wood processing; and sugar cane bagasse. Food processing tertiary residues include: orange and potato peelings; and large quantities of water containing various amounts of proteins, starches, and sugars. Animal operations that produce dairy products, eggs, and meat generate a large stream of residues (at ever increasing scales) from large feedlot operations. These are becoming regulated as concentrated animal feed operations (CAFO)s. These tertiary residues are usually high moisture and most often are treated by a process of anaerobic digestion to produce biogas, a mixture of methane and carbon dioxide, as fuel.

Much of the post consumer residues are in fact biomass: paper, packaging, crates, pallets, demolition lumber, food scraps, and sewage treatment residues. These are more and more often entering the bioenergy, biofuels, and bioproducts stream as society practices resource conservation and use. The Environmental Protection Agency's (EPA) preferred method is source reduction, which includes reuse, followed by recycling and composting, and, lastly, disposal in combustion facilities and landfills.

These primary, secondary, tertiary, and post consumer pathways are significant when compared with the US TPES of about 100 EJ. The total forest harvest is on the order of 203 M tonnes of air-dried round wood equivalents per year, which corresponds to > 3.5 EJ of primary energy equivalent. In recent years the annual corn harvest of almost 10 billion bushels (254 Mt) corresponds to over 4 EJ of primary energy equivalent produced on 3,000 km² (about 75 million acres, or about half of the arable crop area of the USA). Though corn stover is partly required to remain on the land to maintain fertility and reduce soil erosion, the quantity available is similar to the amount of crop and represents the largest agricultural residue potential.

Effect of Transportation on Cost

The key determinant of the feasibility of biomass is the cost of the biomass that contains the stored "free" solar energy. As the cost varies with the transportation distance from the process plant to the field or forest, as well as the opportunity cost of the feedstock, the cost is usually obtained from a supply curve. There are many factors that go into deriving the supply curve for the resource. Due to the bulk of biomass, its transportation over long distances by road is not economical, though with low cost transportation by rail, the distance can be increased. While an 80 km collection is often cited, this is only an order of magnitude. In each case, the actual collection radius will be a function of the biomass density per unit area, the nature of the terrain, road network density, and the condition and type of transportation available.

Density Relationship

One of the highest biomass densities is, in fact, the post consumer residue production of the urban areas. Cities draw upon the resources of vast areas and concentrate them in a small area resulting in a "footprint" that is much greater than the physical urban area. A useful number is a *per capita* urban residue energy generation rate of about 22 MJ *caput*⁻¹ d⁻¹ (1.86 kg d⁻¹ of residue with 11.6 MJ kg⁻¹ heat of combustion, 1990). Major metropolitan areas have population densities of greater than 2000 person km⁻². For this population density, the thermal energy equivalent in their residues is about 4.4 GWh km⁻². If a short rotation woody crop was grown at yields of 15 tonne ha⁻¹ y⁻¹, it would produce about 7.8 GWh km⁻².

Conclusion

The predicted 2020 potential of biomass costing less than 4 \$ GJ⁻¹ is about 8 EJ. The sources and constraints on the biomass resources contributing to this total will be discussed.

BIOMASS PYROLYSIS FOR DISTRIBUTED ENERGY GENERATION

Michael A. Serio, Erik Kroo, and Marek A. Wójtowicz

Advanced Fuel Research, Inc.,
87 Church Street, East Hartford, CT 06108 USA

Introduction

Renewable sources of energy can include solar, wind, ocean tides or temperature gradients, and biomass. However, biomass is the only renewable energy source that is capable of displacing significant amounts of solid, liquid, and gaseous fossil fuels. The historical energy consumption patterns in the U.S. indicate that wood was the dominant energy source for most of the 1800's, followed by coal in the late 1800's and early 1900's and oil and gas in the latter part of the 1900's [1]. In the future, it is likely that the dominance of fossil fuels will gradually diminish in favor of renewable sources of energy, including biomass.

Examples of candidate biomass feedstocks include wood residues and byproducts (e.g., wood chips, sawdust, tree prunings), agricultural residues and byproducts (e.g., corn stover, bagasse, rice husks) or dedicated energy crops (e.g., fast-growing trees, shrubs and grasses) [2]. An important potential source of biomass feedstocks, that is often overlooked, are the livestock and poultry manures, which are generated in significant quantities in the U.S. [2-5].

Besides landfill disposal, many different processes have been considered for utilizing biomass wastes: combustion (incineration), aerobic and anaerobic biodegradation, wet oxidation, supercritical oxidation, steam reforming, etc. [3]. However, all of these approaches have disadvantages which have prevented their widespread use. For example, combustion produces undesirable byproducts such as oxides of sulfur and nitrogen. A staged pyrolysis process has several advantages when compared to other possible approaches: 1) it can be used for all types of solid products and can be more easily adapted to changes in feedstock composition than alternative approaches; 2) the technology is relatively simple and can be made compact and low cost; 3) it can produce several usable products from solid waste streams (e.g., H_2 , CH_4 , CO , liquid fuels, fertilizers, activated carbon, etc.); 4) the technology is environmentally friendly (low net emissions of CH_4 , CO_2 , SO_2 , NO_x , HAP's, VOC's); 5) it can be integrated into microturbine, fuel cell or thermophotovoltaic (TPV) systems for power generation. The main disadvantage of pyrolysis processing is that the product stream is more complex than for many of the alternative treatments. While many pyrolysis studies have been done on biomass materials, most of these have focused on production of liquid fuels, chemicals, or hydrogen [6-8], and not fuel gas mixtures (H_2 , CO , CH_4).

Pyrolysis Processing of Waste Materials

The word *pyrolysis* has its roots in Greek, $\piυρ$ meaning fire, and $\lambdaυσις$ meaning to loosen or untie. Pyrolysis is, therefore, a process of thermal decomposition to produce gases, liquids (tar) and char (solid residue). Pyrolysis is usually understood to be thermal decomposition which occurs in an oxygen-free atmosphere, but oxidative pyrolysis is nearly always an inherent part of combustion processes. Gaseous, liquid and solid pyrolysis products can all be used as fuels, with or without prior upgrading, or they can be utilized as feedstocks for chemical or material industries. The types of materials which are candidates for pyrolysis processes include plant biomass, human and animal wastes, food scraps, crop residues, prunings, paper, cardboard, plastics, rubber [9-11]. These products are primarily polymeric in nature and pyrolysis represents a method

of processing all of these materials into useful products. In the case of plant biomass, human and animal wastes, food scraps, paper and cardboard, pyrolysis can be used to produce fuels or chemicals in gaseous and/or liquid form. In the case of plastics and rubber, pyrolysis can sometimes be used for "recycling" previously manufactured materials back to monomers. Of course, pyrolysis has been used for over 100 years in the processing of coal in coke ovens [9]. Before the large oil discoveries in the Middle East, the chemical industry was largely based on byproducts from the coking process. Advanced Fuel Research, Inc. (AFR) recently completed a study which indicated that pyrolysis of used tires could be an economical way to dispose of this troublesome solid waste stream and, at the same time, produce valuable products [11]. There are several excellent reviews of the biomass pyrolysis literature [1,12-19]. Commercial processes for pyrolysis of plastics and biomass have been developed [1,6-8,9-10]. Most of these have focused on the production of liquid fuels, chemicals, or hydrogen, and not fuel gas mixtures, which are usually considered less valuable.

A recently proposed AFR scheme [20-22] for the pyrolysis processing of spacecraft wastes is shown in Figure 1. In many respects, this scheme is analogous to a "solid waste refinery" and a similar approach could be used for most types of biomass waste in terrestrial applications. The waste stream is heated in the absence of oxygen to temperatures between 673 and 873 K. Thermal decomposition occurs, producing a mixture of liquids (0-50%), gases (30-80%), and a solid residue (20-35%). The initial pyrolysis products are primarily liquids, but these liquids are easily cracked to gases (and small amounts of carbon) as the temperature is raised an additional 100-200 K. The major gas products are H_2 , CO , H_2O , CO_2 , CH_4 . Other gas products, present in much smaller amounts, will include N_2 , NH_3 and H_2S , since nitrogen and/or sulfur compounds are present in most solid wastes. The liquids will initially include a large yield of a complex mixture of chemicals, including levoglucosan and glycoaldehyde for cellulosic wastes. This characteristic of the pyrolysis of waste streams allows for the possibility of staging the pyrolysis process. The initial stage will convert the solids to liquids and will significantly reduce the volume of the waste. In the second stage, the liquids are cracked almost completely to gases. Subsequently, the char residue can be gasified or combusted and the minerals can be recovered for later disposal or use as fertilizer or blended with concrete. The char residue will typically be less than 20% of the initial mass of the solid waste, unless there is a high inorganic content, in which case it could be as high as 35%. The gas stream will need to be cleaned to remove NH_3 and/or H_2S and then the gas can be sent to an energy conversion device (e.g., microturbine, incinerator, TPV or a fuel cell).

A significant advantage of pyrolysis processing is that these stages can be separated in time by minutes, days, or weeks, depending on the demand for the products that are being recovered from the waste. For example, adjusting the pyrolysis conditions to produce primarily liquids will significantly reduce the waste storage volume without significantly increasing the volume of gases that must be used, stored, or discarded. The char residue can also be saved for disposal rather than gasified to simplify the system operation, which may be desirable in certain installations. Alternatively, two systems can be operated in tandem, one in pyrolysis mode and one in gasification mode and the resultant gas streams can be blended to give a more constant off-gas composition. Another possibility would be to use a continuous flow reactor system such as a moving bed, fluidized-bed, or transport reactor. Direct combustion does not allow such a fine degree of control of the outcome and will convert all of the nitrogen to NO_x , an undesirable

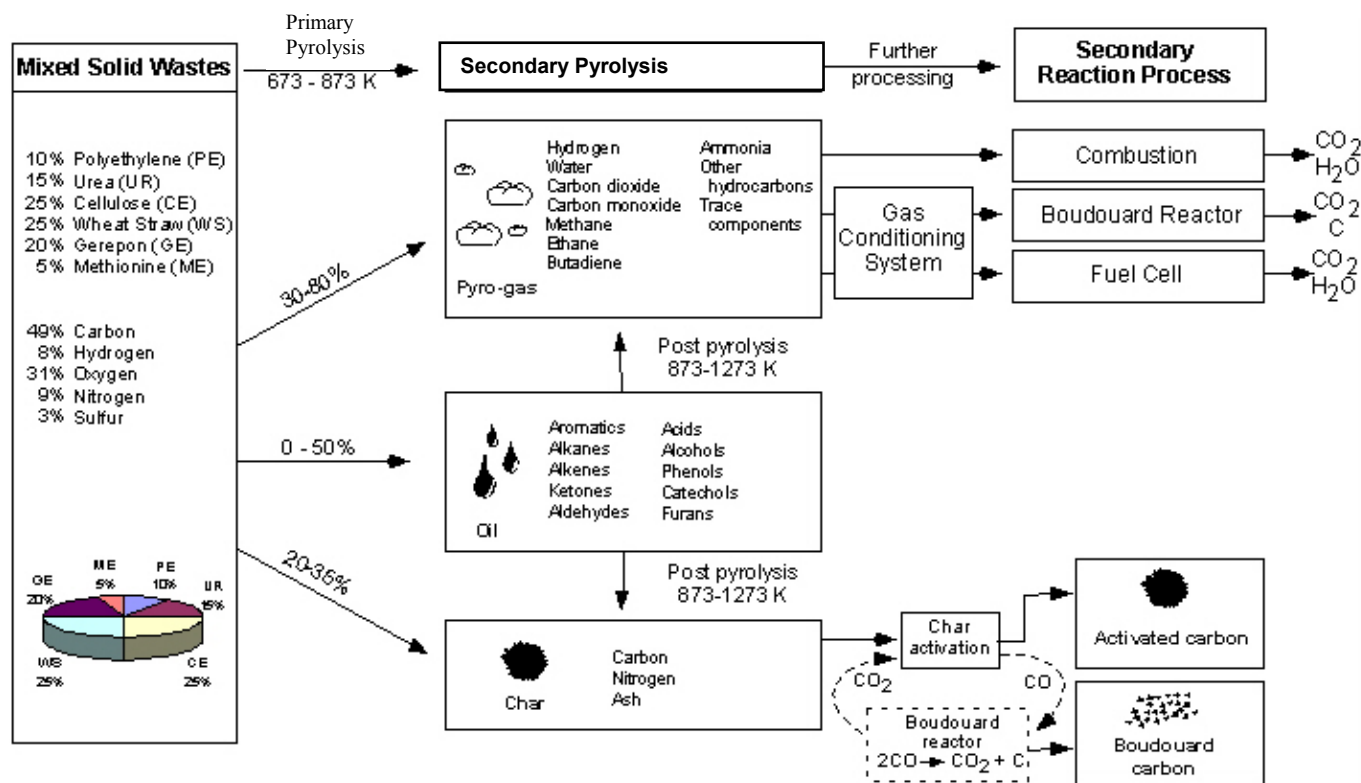


Figure 1. Pyrolysis processing scheme for Controlled Ecological Life Support System (CELSS).

product. In addition, most direct combustion systems will be adversely affected by the high mineral matter contents in many biomass materials. Direct gasification of the biomass wastes will produce a fuel gas with a lower heating value, since the hydrocarbons like CH_4 will be lost.

Experimental Methods

An extensive set of pyrolysis experimental studies at AFR has utilized a TG-FTIR instrument (thermogravimetric analysis combined with FT-IR analysis of evolved products). The application of TG-FTIR to coal analysis at AFR has been described in several publications [23-27]. By using a range of heating rates, kinetic rate constants for volatiles evolution have been obtained [26]. TG-FTIR analysis has also been used at AFR to characterize other hydrocarbon materials such as modified coal samples, [28] coal liquefaction resids [29], petroleum source rocks, [30] lubricants, [31] biomass, [32-35] waste tires, [36] and polymers [37]. This section will briefly review the use of the TG-FTIR technique at AFR for the study of biomass pyrolysis.

Details of the TG-FTIR method can be found in reference [23]. The apparatus consists of a sample suspended from a balance in a gas stream within a furnace. As the sample is heated, the evolving volatile products are carried out of the furnace directly into a 5 cm diameter gas cell (heated to 150 °C) for analysis by FT-IR. In a typical analysis procedure, a 35 mg sample is taken on a 30 °C/min temperature excursion in helium, first to 80 °C to dry, then to 900 °C for pyrolysis. After cooling, a small flow of O_2 is added to the furnace, and the temperature is ramped to 700 °C (or higher) for oxidation (or gasification). During this excursion, infrared spectra are obtained once every forty-one seconds. The spectra show absorption bands for several gases, including CO , CO_2 , CH_4 , H_2O , C_2H_4 , HCl , NH_3 , and HCN . The spectra above 300 °C also show aliphatic,

aromatic, hydroxyl, carbonyl and ether bands from tar (heavy liquid products). The evolution of gases and tars derived from the IR absorbance spectra are obtained by a quantitative analysis program.

The TG-FTIR method provides a detailed characterization of the gas and liquid compositions and kinetic evolution rates from pyrolysis of materials under a standard condition (usually 30 °C/min). While the heating rates are slower than what will be experienced in most practical processes, it is a useful way of benchmarking materials. The ultimate analysis data for several biomass materials that have been studied using the TG-FTIR approach are given in Table 1. The typical TG-FTIR results from pyrolysis at 30 °C/min for these materials are given in Table 2. AFR has developed kinetic models based primarily on TG-FTIR data which can be extrapolated over a wide range of conditions. The TG-FTIR apparatus can also be used to study the reactivity of the pyrolysis residue (char) by introducing appropriate gases. Finally, a secondary reaction zone can be added to examine secondary pyrolysis of the volatile products. These secondary reactions are important in order to maximize the fuel gas production from biomass materials. Additional details can be found in Refs. 32-35.

In recent work, AFR has been involved in building and testing larger scale pyrolysis reactors with NASA support that could be used for solid waste resource recovery in space [20-22]. That project is studying the pyrolysis of mixed solid waste streams, including paper, soap, plastic, and inedible plant biomass, which are relevant to long term space travel.

A schematic of the NASA prototype reactor system is shown in Figure 2. During the initial processing step, the first stage is the primary pyrolysis zone, for thermal decomposition of the sample into gases, liquids and a char residue, while the second stage contains a catalyst bed for decomposition of the liquids. Each of these stages are heated independently (~673-873 K for the first stage, 873-1273 K for

the second stage). During the second-processing step, the purge gas is switched to CO₂ (or H₂O) and gasification of the char can occur in the first stage (if desirable) while gasification of the carbon deposits from the cracked oils will occur in the second stage. Alternatively, the conditions in the first stage can be adjusted to provide activation of the char or no reaction at all, in which case the char can be

removed and used for some other purpose. A picture of the current prototype the reactor is shown in Figure 3. It is anticipated that a suitably modified system could be used in terrestrial applications to produce fuel gases for distributed power generation.

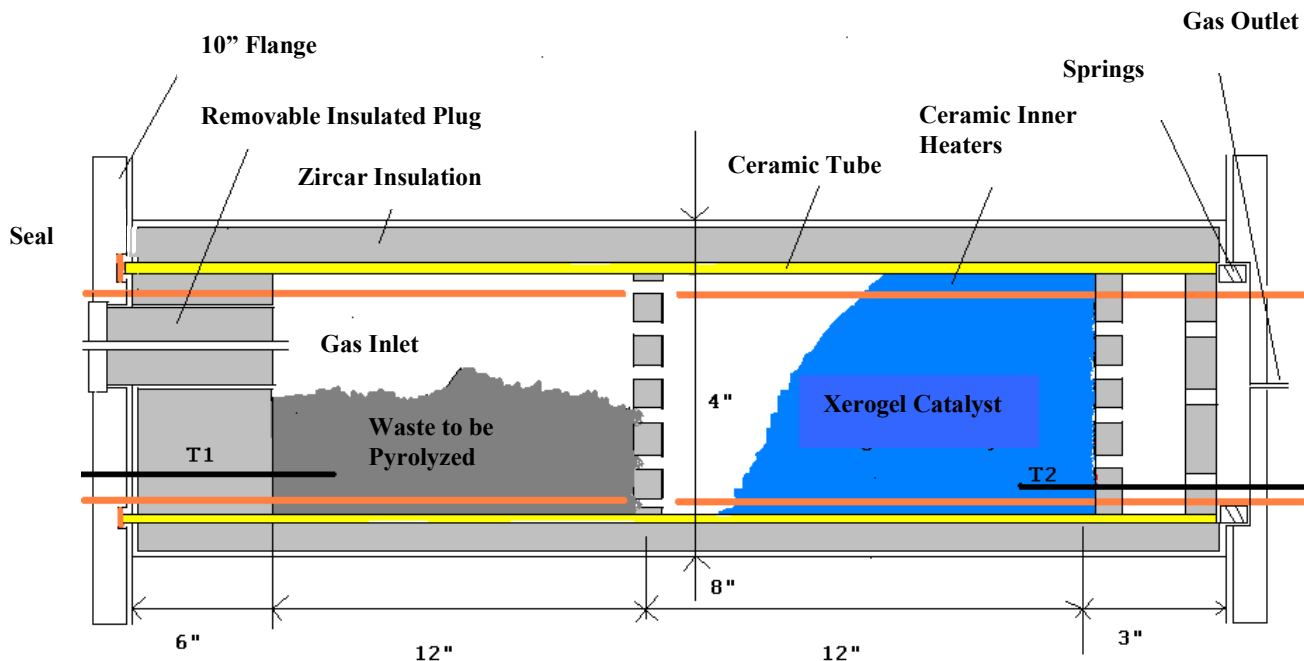


Figure 2. Schematic of First Generation Unit (FGU) two-stage pyrolysis reactor system.

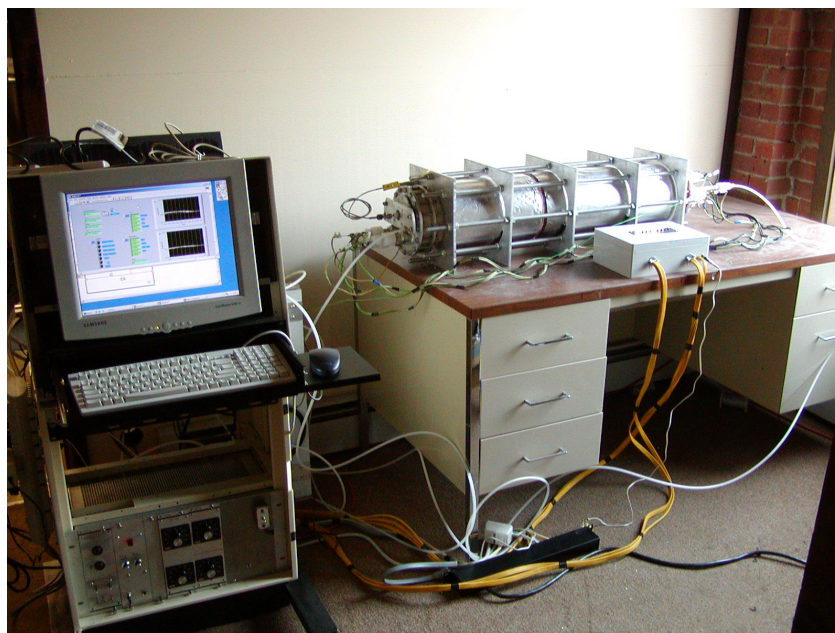


Figure 3. Picture of AFR Prototype Pyrolyzer and Control Console

Table 1. - Ultimate analysis of biomass samples

Sample	Chicken Manure ^a		Lignin ^b		Wheat Straw ^c		Miscanthus Giganteus ^d		Cellulose ^e		Xylan ^f		Wood Pellets ^g	
	AR	DAF	AR	DAF	AR	DAF	AR	DAF	AR	DAF	AR	DAF	AR	DAF
Moisture	11.4		1.9		7.9		8.7		5.0		11.0		8.2	
Ash	20.0		0.0		8.3		2.5		0.0		3.6		0.3	
C		47.4		67.4		48.0		49.4		44.0		45.0		52.1
H		6.5		6.2		6.2		5.5		6.2		6.0		5.2
O		39.5		26.2		44.9		44.0		49.8		48.9		42.2
S		1.0		0.0		0.2		0.2		0.0		0.0		0.1
N		5.6		0.2		0.7		0.6		0.0		0.0		0.3

Notes: AR = As-received; D=Dry; DAF=Dry, Ash Free

a-Plant Right (Purdy, MO); b- ALCELL Technologies, Inc., (Valley Forge, PA (ADI/L952)); c- NIST, (Gaithersburg, MD); d-Delft University of Technology; e- Avicel (pH-102/Lot 2822); f- Philip Morris USA; g - Labee Company, the Netherlands.

Table 2. Results from TG-FTIR experiments at 30 °C/min for various biomass samples

Sample	Chicken Manure	Lignin	Wheat Straw	Miscanthus Giganteus	Cellulose	Xylan	Wood Pellets
Moisture	11.2	1.9	7.5	2.5	12.4	9.5	6.3
Ash	18.3	0.0	7.9	3.8	0.0	2.0	0.0
Volatile Matter	59.1	69.5	68.0	74.4	85.3	67.6	80.8
Fixed Carbon	11.4	29.2	16.6	19.3	2.3	21.0	12.9
Tars	28.5	39.5	35.1	21.9	81.5	13.3	38.8
CH ₄	0.98	2.40	1.20	1.14	0.13	0.87	1.3
H ₂ O (pyr)	18.7	7.6	21.8	18.4	5.1	24.2	16.0
CO ₂	14.3	1.9	14.5	9.4	2.0	15.9	5.1
CO	6.37	6.50	9.26	7.15	1.49	9.64	6.77
C ₂ H ₄	0.25	0.22	0.26	0.27		0.42	0.23
SO ₂	0.08		0.36	0.00		0.12	0.12
COS	0.61		0.23	0.16			0.11
NH ₃	1.91		0.18	0.10			0.02
HCN	1.21	0.04	0.25	0.14	0.03	0.15	0.09
Formic Acid	0.72		1.61	1.66	0.34	1.75	1.73
Acetic Acid	1.63		5.52	3.59	0.57	2.65	2.37
CH ₃ OH	0.10	2.20	1.21	1.12	0.75	1.72	0.74
Formaldehyde	0.00	0.22	0.92	1.12	1.23	0.45	2.93
Acetaldehyde	6.31	1.55	8.62	9.02			8.11
Acetone	1.04	3.91	2.38	1.86			2.15

Notes: Yields are given on wt.% dry, ash-free basis except for moisture, ash, volatile matter, and fixed carbon which are given on an as-received basis.

Application to Distributed Power Generation

In the past few years, the level of commercial interest in distributed power generation has increased dramatically. According to recent data, the amount of venture capital investment in "micropower" technology has increased from \$100 million in 1996 to \$200 million in 1998 and an estimated \$800 million for 2000 [38]. Fuel cell systems that are currently commercial operate at relatively low temperatures and use pure hydrogen as a fuel [39]. Examples are the phosphoric acid system and the polymer electrolyte membrane (PEM) systems. In order to use these cells with a fuel gas which

contains CH₄, CO, and H₂, a reformer and shift converter must be used. However, also under development are high temperature fuel cells (HTFC) which have molten carbonate (MCFC) or solid oxide electrolytes (SOFC). The latter fuel cells are especially interesting for combination with a biomass pyrolysis process, since these can tolerate a mixture of CO, CH₄, and H₂, and operate at temperatures ranging from 650 °C to 1000 °C. This high temperature heat could be used to help drive the pyrolysis and char gasification reactors and/or provide heat for building operations. Some of these HTFC systems have been successfully operated on landfill gas and digester gas,

which produce similar gas streams to the fuel gas that is produced from biomass pyrolysis.

Thermophotovoltaic (TPV) systems are also of interest because they can operate on fuel gases which contain mixtures of H₂, CH₄, and CO. These systems involve using the radiant energy from a flame to produce electricity from specially designed photovoltaic cells. TPV systems are also lower in cost and closer to commercialization than the HTFC's. A company in the Pacific Northwest (JXCystals) is marketing TPV generation equipment for residential and mobile uses [40]. The military is also sponsoring the development of TPV systems for mobile power generation units.

A third possibility, which has near term potential, is to couple the pyrolysis process with a microturbine, such as those produced by Capstone Turbine Corp (Chatsworth, CA). These systems are much cheaper when compared to fuel cell and TPV systems and are already available in significant quantities at appropriate power generation rates. Approximately the size of a large refrigerator, Capstone's Model 330 Microturbine generates approximately 30 kilowatts of electrical power which is enough power to power a convenience store, and approximately 300,000 kilojoules per hour of heat, enough energy to heat 20 gallons of water per minute with a 20 degree heat rise. The Capstone Microturbine can operate connected to the electric utility grid or on a stand-alone basis. It remains to be seen how well microturbines can operate on hydrogen-rich fuel gas streams.

Summary

The conversion of fuel gases from biomass pyrolysis to power using either a fuel cell, TPV or microturbine system would provide numerous technical, economic, and social benefits:

- It would remove biomass from landfills where they take up valuable space and decompose to produce CH₄ and CO₂, both greenhouse gases.
- It would provide a means of generating power in remote agricultural areas, a benefit from an economic and quality-of-life standpoint to both farms in the U.S. and in underdeveloped nations.
- It would provide a means of generating off-grid power in business and residential applications where significant quantities of biomass wastes (e.g., paper, food residues) are readily available.
- The power generated would most likely replace power produced at central power stations and diesel generators from fossil fuels, thus providing a net reduction in CO₂, NO_x, and SO₂.

The technology would contribute to and benefit from the expected growth in the emerging distributed power generation industries over the next several years. Challenges remain in reducing the costs of the next generation power generation equipment and in economical production of clean fuel gases from biomass pyrolysis. It is likely that early demonstration projects will require tax incentives in order to compete with conventional power generation equipment utilizing fossil fuels.

Acknowledgements.

AFR has received support for biomass pyrolysis R&D from the NASA-Ames Research Center under contracts NAS2-99001 and NAS2-00007, which is gratefully acknowledged. The COTR was John Fisher. AFR has also received support for biomass pyrolysis studies from the University of Florida Environmental Systems Commercial Space Technology Center (William Sheehan, Project Director) and Philip Morris USA (Mohammad Hajaligol, Project Director). In addition, we would like to acknowledge support from the U.S. DOE under contract DE-FG02-00ER82936 for the pyrolysis experiments with chicken manure. Prof. Eric Suuberg of Brown

University has been a consultant or collaborator on many of AFR's biomass pyrolysis projects.

References

- 1 Klass, D.L., "Biomass for Renewable Energy, Fuels, and Chemicals," Academic Press (1998).
- 2 Barrier, T.W., and Bulls, M.M., "Feedstock Availability of Biomass and Wastes," Chapter 23, in ACS Symposium Series No. 476, ACS Washington, DC pp. 410-421.
- 3 Chartier, P., Ferrero, G.L., Henius, V.M., Hultberg, S., Sachau, J., Wiinblad, M., "Biomass for Energy and the Environment," Pergamon, New York (1997).
- 4 Stanford Research Institute, "An Evaluation of the Use of Agricultural Residues as an Energy Feedstock," Vol. 1, NSF Grant No. AER74-18615 A03 (1976).
- 5 Gerwig, B.K., Hegg, R.D., "Assessment and Characterization of Manure in the Southeast U.S.," Proceedings of Bioenergy '96, pp. 501-507, Sept. 15-20, 1995.
- 6 Rowell, R.M., Schultz, T.P., Narayan, R., "Emerging Technologies for Materials and Chemicals from Biomass," ACS Symp. Series No. 476, ACS Books, Washington, DC (1992).
- 7 Dayton, D.C., Chum, H.L., "Symposium on Biomass Fuels: The Introduction," Energy & Fuels, 10 (2), 267 (1996).
- 8 Wang, D., Czernik, S., Montané, D., Mann, M., Chornet, E., Ind. Eng. Chem. Res., 36, 1507 (1997).
- 9 Serio, M.A., Wójtowicz, M.A. and Charpenay, S., "Pyrolysis," In Encyclopedia of Energy Technology and The Environment, (A. Bisio and S.G. Boots), John Wiley & Sons, New York, NY, 2281-2308 (1995).
- 10 Bridgwater, A.V., Biomass, 22, (1-4), 279 (1990).
- 11 Wójtowicz, M.A. and Serio, M.A., Chemtech, 26, (10), 48-53 (1996).
- 12 Antal, M.J., Jr., in Adv. in Solar Energy (Boer, K.W., Duffie, J.W., Eds.), American Solar Energy Society, Boulder, CO, 1, 61 (1984); 2, 175 (1985).
- 13 Soltes, E.J., in Biomass Energy Development, W.H. Smith, Ed., Plenum Press, New York, 321 (1986).
- 14 Shafizadeh, F., in The Chemistry of Solid Wood (R. M. Rowell, Ed.), Advances in Chemistry Series No. 207, American Chemical Society, Washington, DC (1984).
- 15 Bridgwater, A.V., and Cottam, M.-L., Energy and Fuels, 6, (2), 113 (1992).
- 16 Elliott, D.C., Beckman, D., Bridgwater, A.V., Diebold, J., Severt, S.B., and Solantusta, Y., Energy and Fuels, 5, 399 (1991).
- 17 Overend, R. P. Milne, T. A., and Mudge, L.K., Eds., Fundamentals of Thermochemical Biomass Conversion, Elsevier, (1985).
- 18 Soltes, E.J., and Milne, T.A., Eds., Pyrolysis Oils from Biomass: Producing, Analyzing and Upgrading, ACS Symposium Series No. 376, American Chemical Society, Washington, DC (1988).
- 19 Bridgwater, A.V., Kuester, J.L., (Eds.), Research in Thermochemical Biomass Conversion, Elsevier Applied Science, London (1988).
- 20 Serio, M.A., Chen, Y., Wójtowicz, M.A. and Suuberg, E., "Pyrolysis Processing for Solid Waste Resource Recovery in Space," 30th International Conference on Environmental Systems, Toulouse, France July 10-13, 2000. SAE Paper No. 2000-01-2286.
- 21 Serio, M.A., Kroo, E., Bassilakis, R., Wójtowicz, M.A., and Suuberg, E.M., "A Prototype Pyrolyzer for Solid Waste

- Resource Recovery in Space,” 31st International Conference on Environmental Systems, Orlando, FL, July 9-12, 2001, SAE paper No. 2001-01-2349.
- 22 Serio, M.A., Kroo, E., Wójtowicz, Suuberg, E., and Filburn, T., “An Improved Pyrolyzer for Solid Waste Resource Recovery in Space,” 32nd International Conference on Environmental Systems, San Antonio, Texas, July 15-18, 2002, SAE Paper No. 2002-01-2402.
 - 23 Carangelo, R.M., Solomon, P.R., and Gerson, D.G., *Fuel*, 66, 960 (1987).
 - 24 Solomon, P.R., Serio, M.A., Carangelo, R.M., Bassilakis, R., Gravel, D., Baillargeon, M., Baudais, F., and Vail, G., *Energy & Fuels*, 4, (3), 319 (1990).
 - 25 Solomon, P.R., Serio, M.A., Carangelo, R.M., Bassilakis, R., Yu, Z.Z., Charpenay, S., and Whelan, J., *Journal of Analytical and Applied Pyrolysis*, 19, 1 (1991).
 - 26 Solomon, P.R., Hamblen, D.G., Serio, M.A., Yu, Z.Z., and Charpenay, S., *Fuel*, 72, (4), 489 (1993).
 - 27 Bassilakis, R., Zhao, Y., Solomon, P.R. and Serio, M.A., *Energy & Fuels*, 7, 710 (1993).
 - 28 Charpenay, S., Serio, M.A., Bassilakis, R., and Solomon, P.R., *Energy & Fuels*, 10, 19 (1986).
 - 29 Teng, H., Serio, M.A., Bassilakis, R., Knight, K.S., Bates, S.C., and Solomon, P.R., *ACS Fuel Chem. Preprints*, 37, (4), 1903 (1992).
 - 30 Whelan, J.K., Solomon, P.R., Deshpande, G.V., and Carangelo, R.M., *Energy and Fuels*, 2, 65 (1988).
 - 31 Bonanno, A.S., Bassilakis, R., and Serio, M.A., *ACS Fuel Chem. Preprints*, 41(1), 62 (1996).
 - 32 Serio, M.A., Kroo, E., Bassilakis, R., Solomon, P.R., and Malhotra, R., *ACS Fuel Chem. Preprints*, 36, (3), 1110 (1991).
 - 33 Serio, M.A., Charpenay, S., Bassilakis, R., and Solomon, P.R., *Biomass & Bioenergy*, 7, (1-6), 104 (1994).
 - 34 Bassilakis, R., Carangelo, R.M., and Wójtowicz, M.A., “TG-FTIR Analysis of Biomass Pyrolysis,” *Fuel*, 80, 1765-1786 (2001).
 - 35 de Jong, W., Pirone, A., and Wójtowicz, M.A., “Pyrolysis of *Miscanthus Giganteus* and Wood Pellets: TG-FTIR analysis and reaction kinetics,” *Fuel*, 82, 1139-1147 (2003).
 - 36 Teng, H., Serio, M.A., Wójtowicz, M.A., Bassilakis, R., and Solomon, P.R., *Industrial & Engineering Chemistry Research*, 34, 3102 (1995).
 - 37 Serio, M.A., Charpenay, S., Bassilakis, R., and Solomon, P.R., *ACS Div. of Fuel Chem. Preprints*, 36, (2), 664 (1991).
 - 38 “The Dawn of MicroPower,” *Economist*, pp. 75-77, August 5, 2000.
 - 39 Appleby, T., “Fuel Cells” in the *Wiley Encyclopedia of Energy and the Environment*, Wiley, New York, pp. 783-796 (1997).
 - 40 Cougs, T.J., Fitzgerald, M.C., “Thermophotovoltaics,” *Scientific American*, pp. 90-95 (Sept. 1998).

BIOMASS TORREFACTION STUDIES WITH A MOLECULAR BEAM MASS SPECTROMETER

Mark N. Nimlos, Emily Brooking, Michael J. Looker, and Robert J. Evans

National Bioenergy Center
National Renewable Energy Laboratory
Golden, Colorado 80401

Introduction

An important drawback to using biomass as fuel source is the fact that its energy density is much lower than that of traditional energy resources such as fossil fuels. This low density makes biomass fuel more expensive to transport, store and utilize than fossil fuel. This problem is compounded by the hydrophilic nature of the material. The absorption of moisture causes the biomass to decrease in energy density even further and make its use even more expensive and less feasible on a massive scale.

Torrefaction¹⁻⁶ is a technique to improve the energy content of biomass, which involves the heating of biomass to moderate temperatures (200-300 °C). At these temperatures, chemically bound water can be released from the biomass, increasing the carbon content and the heat of combustion. There is also the benefit that the biomass becomes more hydrophobic after torrefaction. This can be particularly important for energy densification or pellet making. Finally, there is the possibility that torrefaction could be used to increase the density of biomass pellets.

We have conducted torrefaction experiments with hardwood sawdust to measure the increase in energy content and to investigate the effect upon pellet making. We have torrefied the wood at a variety of temperatures (175–295 °C) and residence times (5–30 min.). Weight loss and heat of combustion of the resulting powder were measured. We also used a pyrolysis mass spectrometer and factor analysis to identify changes in the wood. Finally, we have used a high pressure press to prepare of pellets from torrefied wood.

Experimental

The sample material used in this research was Vermont hardwood sawdust which was prepared by grinding pellets. Small samples (100 – 200 mg) of the sawdust were placed in 5 cm ceramic boats and slid into a heated tubular reactor held at the desired temperature by a tube furnace. A small flow of nitrogen gas (0.5-1.5 L/min.) was provided to remove liberated species from the reactor. Under these conditions heat transfer effects were minimized as evidenced by the uniformity of color of the torrefied wood. The temperature of torrefaction was controlled using a thermocouple placed next to the samples in the furnace.

Pelletization was accomplished with a hydraulic laboratory press (Carver) with heated platens. The dies used in pelletization were Carver hardened stainless steel dies rated up to a 18,000 lb load with a .5 inch interior diameter. A 10,000 lb load was applied to each pellet.

In order to investigate the change in chemical composition, pyrolysis mass spectra of the torrefied samples were collected. The pyrolysis products from these samples were measured using a molecular beam mass spectrometer^{7, 8} (MBMS). Small samples (~20 mg of the torrefied wood were inserted into a flow of hot (550°C) helium and the products were carried to the sampling orifice of the MBMS.

Finally, heats of combustion of the samples were measured (Hazen Research, Inc) using bomb calorimetry.

Results and Discussion

Weight loss

During torrefaction, the wood samples change color from a light brown (without heating) to a dark brown at the higher temperatures. **Figure 1** shows a contour plot of the measured weight loss as a function of temperature and residence time in the oven. As can be seen, temperature has a more profound effect upon the weight loss than residence time.

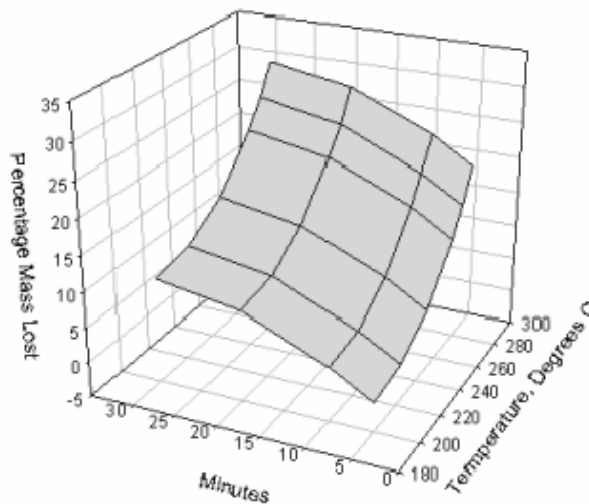


Figure 1. A contour plot of the measured weight loss versus the temperature and residence time of torrefaction.

Pellet density

Pellets made from the untreated and torrefied wood were often somewhat flaky though the pellets made from torrefied wood were typically less so. We made three pellets of each sample and compared the density. Within the uncertainty of our measurements, we found no change in the density of the pellets with torrefaction. When the platens of the press were heated, we typically form more dense pellets with less flaking. Because of experimental limitations, we did not systematically study this effect.

MBMS analysis

Pyrolysis MBMS data was collected for all of the torrefied samples as well as untreated sawdust. Typical mass spectra obtained from these experiments is shown in **Figure 2**. The pyrolysis mass spectra for the untreated sawdust contains peaks for lignin's primary pyrolysis components ($m/z = 210, 194$ and 180) and hemicellulose pyrolysis components ($m/z = 114$ and 85). The spectra from the most severe condition studied (295 °C, 30 min. residence time) shows peaks for secondary lignin products ($m/z = 168$ and 154) and products from cellulose pyrolysis ($m/z = 126$ and 110).

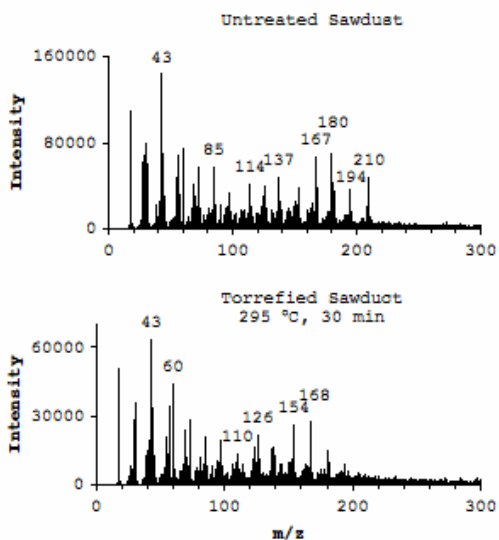


Figure 2. Pyrolysis mass spectra of untreated sawdust and sawdust torrefied at 295 °C for 30 min.

Factor analysis allows one to extract important trends from the complicated mass spectra obtained during biomass pyrolysis. This analysis was conducted using pyrolysis mass spectra obtained for the entire data set (200–295 °C, 5–30 min) and a clear trend was identified, particularly at higher temperatures. **Figures 3 and 4** show some of the results. We were able to extract two components (or factors) from our analysis. The mass spectra of the components are shown in **Figure 3**. Factor 1 is the primary lignin products and the hemicellulose products and Factor 2 is the secondary lignin products and products from cellulose.

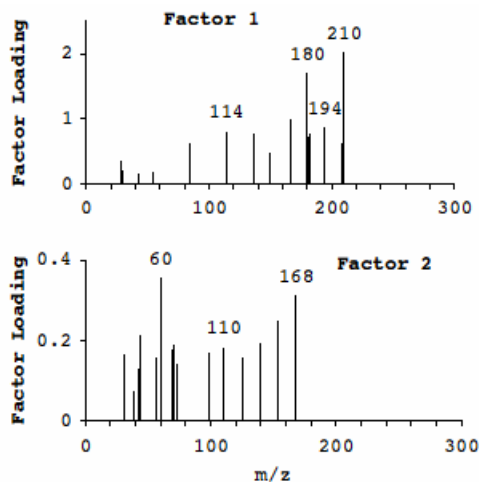


Figure 3. Spectra of correlated products from pyrolysis MBMS experiments of torrefied sawdust samples.

Figure 4 Shows the scores for these factors as a function of residence time of torrefaction at 295 °C. The plot clearly shows that with increasing residence time, factor 1 decreases and factor 2 increases. The decrease in Factor 1 with residence time is accompanied by an increase in weight loss (**Figure 1**). This may be an indication that these components are driven off of the biomass, or it could be that the thermal reactions that lead to volatile products also causes the Factor 1 components to crosslink.

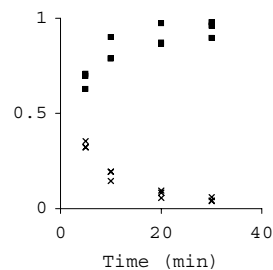


Figure 4 A plot of the scores for factor 1 and factor 2 as a function of the time of torrefaction at 295 °C.

Calorimetry

Table I shows the measure heat of combustion of the torrefied sawdust samples. The measured uncertainty in our measurements is about 200 BTU/lb. The heat of combustion for the untreated sawdust was measured to be 8439 BTU/lb. As can be seen there is not a significant change in the heat as a function of temperature at the lowest residence time (5 min). At the longest residence time (30 min) there is a significant change in heat as the temperature increases.

Table I. Heat of combustion (BTU/lb) of torrefied sawdust on a dry basis

Time (min)	Temperature (°C)					
	200	225	250	275	285	295
5	8521	8546	8512	8496	8609	8397
10	8452	8574	8485	8646	8583	8931
20	8448	8285	8589	8728	9181	8728
30	8741	8669	8780	8716	9308	9494

Acknowledgment

We would like to thank the Department of Energy's Office of Science and NREL's Education Office for making this study possible.

References

- Bourgeois, J.P.D.J., *Torrefied Wood from Temperate and Tropical Species, Advantages and Prospects*, in *Bioenergy 84*, A.E. H. Egnens, Editor. 1985, Elsevier Applied Science: London. p. 153-159.
- F. Fonseca Felfli, C.A.L., P. Beaton, J. A. Suarez. *Efficiency test for bench unit torrefaction and characterization of torrefied biomass*. in *Biomass, Proc. Biomass Conf. Am. 4th*. 1999: Elsevier Science.
- Pentananunt, R., A. Rahman, and S.C. Bhattacharya, *Energy*, 1990. 15(12): p. 1175-1179.
- Bourgeois, J. and R. Guyonnet, *Wood Sci. Technol.*, 1988. 22(2): p. 143-155.
- Bourgeois, J., M.C. Bartholin, and R. Guyonnet, *Wood Sci. Technol.*, 1989. 23(4): p. 303-310.
- Lipinsky, E.S., J.R. Arcate, and T.B. Reed, *Abstr. Pap. Am. Chem. Soc.*, 2002. 223: p. 171-FUEL.
- Evans, R.J. and T.A. Milne, *Energy Fuels*, 1987. 1(2): p. 123-137.
- Shin, E.J., M.R. Nimlos, and R.J. Evans, *Fuel*, 2001. 80(12): p. 1697-1709.

HYDROGEN PRODUCTION BY STEAM REFORMING OF WASTE VEGETABLE OILS

Richard J. French, and Stefan Czernik

National Bioenergy Center
National Renewable Energy Laboratory
1617 Cole Boulevard
Golden, CO 80401

Introduction

Commercially, most hydrogen is produced by steam reforming natural gas, LPG, or naphtha or by partial oxidation of heavy oil fractions. Life-cycle analysis of natural gas steam reforming shows that the amount of fossil CO₂-equivalent released into the atmosphere to produce 100 kg of hydrogen gas is 1374.5 kg.¹ An environmentally preferable alternative is to produce hydrogen from renewable resources, for example via thermal conversion of biomass². In this case the CO₂ released into the atmosphere during thermo-chemical conversion is offset by the uptake of CO₂ during biomass growth. However, direct gasification of lignocellulosic biomass yields less hydrogen than steam reforming of natural gas and so cannot compete with this well-developed technology.³ Therefore, we have studied ways to improve the profitability of hydrogen from biomass by the integrating valuable co-products into the process.⁴

Vegetable oils are derived from biomass and are potentially better hydrogen producers than lignocellulosic materials because the oils contain much less oxygen and more carbon. Sunflower oil, when converted by catalytic steam reforming, yields 25-31 g hydrogen (72% to 87% of the stoichiometric potential (complete conversion to CO₂ and H₂)).⁵ Although the high cost of vegetable oil makes the process economics unfavorable low-cost waste oils, such as "trap grease", are available throughout the country. This grease is recovered from traps in the sewage lines of restaurants and food processing plants and from wastewater treatment plants. Although the bio-diesel industry considers it a potential feedstock, at present trap grease is mostly disposed of. Grease-trap-pumping companies in the Boston area pay tipping fees of 11¢/gallon.

The estimated average amount of recovered waste grease is 13 lbs/person/year.⁶ The U.S.'s trap grease could produce 1 billion pounds of hydrogen annually (0.5 Mtonnes/year). Dewatered grease is available for 2-4 ¢/lb. At this cost, the feedstock contributes only 1-2 \$/GJ to the total cost of hydrogen. With current market prices for hydrogen at 6-9 \$/GJ range, trap grease offers an attractive opportunity for competitive production of hydrogen from renewable resources.

Preliminary reforming tests showed promising results, yielding 30 g of hydrogen from 100 g of grease (81% of the stoichiometric potential) during 17 hours of operation.⁴ Hence, further investigation was warranted. The objective of the work described below was to determine the long-term catalyst efficiency under different operating conditions, as well as identify and suggest solutions to potential problems in the use of waste grease to produce hydrogen.

Experimental

Feedstock. Trap grease was obtained from the DOE Biodiesel Program for whom Pacific Biodiesel collected over 40 samples from different sites in the United States. These contained both saturated and unsaturated C₁₆ and C₁₈ fatty acids, fats, and small amounts of solids (University of Toronto analysis). We selected samples with a high content of free fatty acids (>70%) and low ash (<1%). These were dark colored viscous liquids at room temperature. A batch of 20 kg of such grease was homogenized by heating to 60°C and stirring.

Initial tests were carried out using trap grease as received. However, because of difficulties with feeding (plugging the nozzle), the batch used in the long-duration experiment was washed with hot water and filtered to remove particles. Elemental analysis of this batch showed 75.7%C, 11.9%H, and 13.3%O with 0.05% ash.

Fluidized bed system. The steam reforming experiments were carried out using a bench-scale fluidized bed reactor system. The tubular two-inch-diameter inonel reactor was supplied with a perforated gas distribution plate and was externally heated electrically. The reactor contained 250-280g of commercial nickel-based catalyst (C11-NK) developed by United Catalysts for reforming moderately heavy petroleum fractions. The catalyst had been ground to a particle size of 300-500µ. Before reforming, the catalyst was activated in H₂/N₂ at the process temperature for approximately 2 hours. The reduction of NiO to Ni gave a weight loss of about 7%. The catalyst was then fluidized using superheated steam (750°C), which is also a reactant in the reforming process. The trap grease was continuously weighed and was pumped into the reactor through a temperature-controlled injection nozzle at 60-80°C to provide suitable viscosity. The product collection line included a cyclone and a hot-gas filter to capture fine catalyst particles and, possibly, char generated in the reactor. It also contained two heat exchangers to condense excess steam. The condensate weight was continuously monitored. The outlet gas flow rate was measured *via* a mass flow meter and a dry test meter. The concentrations of H₂, CO₂, CO, and CH₄, C₂H₄, and N₂ in the reformed gas were monitored by infrared (NDIR Model 300 from California Analytical Instruments) thermal conductivity (TCM4 from Gerhard Wagner, Germany) and an MTI micro GC. Temperatures and flows were recorded and controlled by an OPTO22 system.

Results and Discussion

At high temperatures vegetables oils undergo extensive thermal cracking leading to the formation of hydrocarbons. To minimize the extent of the competing thermal decomposition reactions Marquovich *et al.*⁷ carried out catalytic reforming of those oils at 500-650°C. However, complete conversion of the oils to gases was not achieved. In this work on "trap grease" we studied the effect of temperature in the range of 600-850°C. The molar steam-to-carbon ratio (S/C) varied from 2.75 to 5 and the methane-equivalent gas space velocity (G_{C1}VHSV) was in the range of 950-1400 h⁻¹.

At 600°C after 1 hour the concentration of hydrogen in the product gas from "trap grease" reforming started decreasing while that of methane and ethylene rapidly increased rapidly indicating that hydrocarbons were no longer being efficiently converted to hydrogen and carbon oxides. The yield of hydrogen was 70% at the beginning but decreased to 40% of the stoichiometric potential after only 70 minutes of operation. Also conversion of carbon to gas was less than 70%. The remaining 30% probably formed carbon deposits on the catalyst, thus reducing its activity, and larger molecular weight compounds recovered in the condensate.

At higher temperatures and S/C and lower space velocity the catalyst performed much better. At 750°C the carbon to gas conversion was higher than 96% and the yield of hydrogen was above 70% of the stoichiometric potential for 16 hours of operation. At 850°C, S/C=3.5, and G_{C1}VHSV of 1300 h⁻¹ the yield of hydrogen was greater than 80% of the stoichiometric potential and carbon to gas conversion was greater than 99% for six hours.

A long-duration reforming test of washed and filtered "trap grease" was carried out at 850°C, S/C=5, and at the initial G_{C1}VHSV of 970 h⁻¹ (effective space velocity increased during the test due to the progressive catalyst losses from the reactor). Also, similarly to the reforming natural gas, a small amount of hydrogen (<10% of the hydrogen produced) was introduced with the steam to prevent

oxidation of the catalyst. After modest changes during the first 15 hours the gas concentrations remained stable for 120 hours as shown in Figure 1.

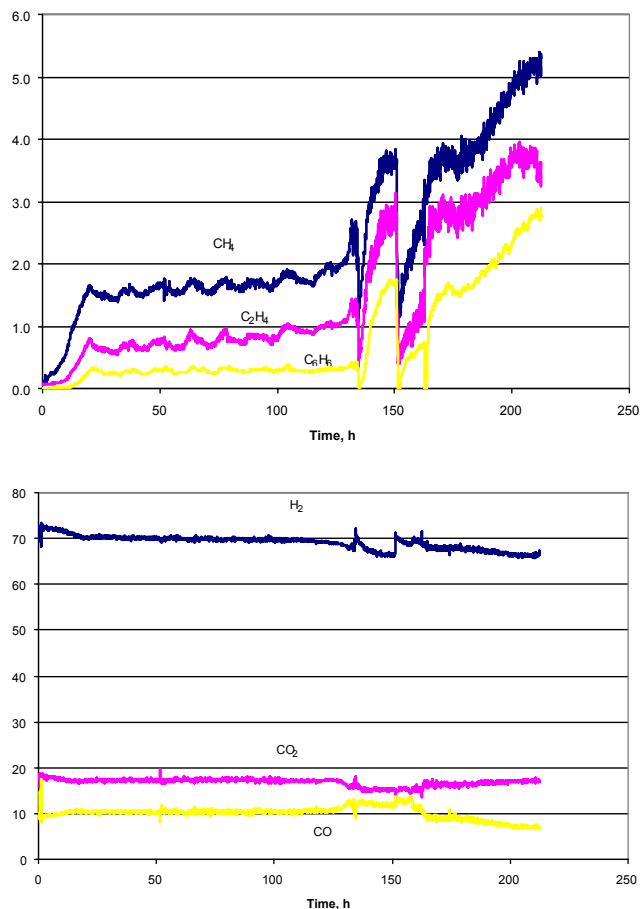


Figure 1. Composition of product gas from reforming of "trap grease," %v/v; $t=850^{\circ}\text{C}$, $S/C=5$, $G_{Cl}VHSV=970\text{ h}^{-1}$.

At 135 hours an upset in feeding interrupted the operation. When the test was restarted a continuous decrease in hydrogen and increase in hydrocarbons was observed during the next 15 hours. We attempted to regenerate the catalyst by steam and hydrogen treatment then continued operation for the combined total of 213 hours. However, performance continuously decreased.

For 135 hours the hydrogen yield was 25 g/100 g grease and could have exceeded 28 g/100 g with the addition of water-gas shift. At the end, this yield decreased to 16.4 g/100 g grease (48% of the stoichiometric potential) as shown in Figure 3. However, throughout the whole experiment the conversion of carbon from grease to gas was 100% with the overall mass balance closure almost 100%. No carbon deposits, nickel sintering, sulfur or other poisons were detected by preliminary thermo-emission electron microscopy (TEM) and ICP analyses on the catalyst, though these remain possibilities.

The main reason for the unsatisfactory performance in the last part of the test was probably the loss of catalyst from the reactor. Out of 280 g of the C11-NK catalyst at the beginning of the experiment (260 g reduced) 65 g remained in the reactor at the end and 165 g of fine material were recovered from the cyclone and filter (30 g missing). Therefore, at the end of the experiment the space velocity was four times greater than initially, overloading the catalyst. The catalyst losses seemed to intensify after 135 hours on

stream, possibly because of flow upsets and weakening of the particles during regeneration.

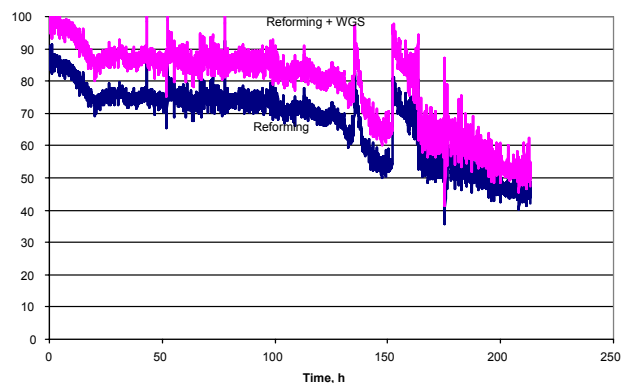


Figure 2. Yield of hydrogen produced by reforming "trap grease," % of ideal stoichiometry; $t=850^{\circ}\text{C}$, $S/C=5$, $G_{Cl}VHSV=970\text{ h}^{-1}$.

Since these catalyst losses are not acceptable, more robust fluidisable catalysts are being produced.⁸ Alternatively, a circulating fluidized bed reactor that would use easier-to-produce smaller ($80\ \mu$) catalyst particles is being considered.

Conclusions

We demonstrated fluidized bed catalytic steam reforming can produce hydrogen from "trap grease", at conditions similar to methane reforming.

The hydrogen yield was about 25 g per 100 g grease (74% of ideal for 135 hours and could be increase to 28 g by water-gas shift of the remaining CO.

Performance deteriorated after 135 hours, probably due to catalyst loss. Therefore, fluidisable attrition-resistant catalysts are being produced and a circulating bed is being considered.

Acknowledgement. We thank Shaine Tyson, manager of the NREL Biodiesel Program for providing the samples of "trap grease" and the grease analysis.

References

- (1) Spath, P. L.; Mann, M. K. Life Cycle Assessment of Hydrogen Production via Natural Gas Steam Reforming. National Renewable Energy Laboratory (NREL), Golden, CO, 2000, TP-570-27637
- (2) Wang, D.; Czernik, S.; Montané, D.; Mann, M.; and Chornet, E. *Ind. Eng. Chem. Res.* **1997**, *36*, 1507.
- (3) Spath, P.; Lane, J.; Mann, M.; Amos, W. Update of Hydrogen from Biomass – Determination of the Delivered Cost of Hydrogen. NREL Process Analysis Task Milestone Report, April 2000.
- (4) Czernik, S.; French, R.; Feik, C.; Chornet, E. *Ind. Eng. Chem. Res.* **2002**, *41*, 4209.
- (5) Marquevich, M.; Coll, R.; Montané, D. *Ind. Eng. Chem. Res.* **2000**, *39*, 2140.
- (6) Wiltsee, G. Urban Waste Grease Resource Assessment, 1998 Report prepared by Appel Consultants, Inc., for NREL, subcontract No. ACG-7-17090-01.
- (7) Marquevich, M.; Medina, F.; Montané, D. *Catalysis Communications* **2001**, *2*, 119.
- (8) French, R.; Magrini-Bair, K.; Czernik, S.; Parent, Y.; Ritland, M.; Chornet, E. *Prepr. Pap.-Am. Chem. Soc., Div. Fuel Chem.* **2002**, *47(2)*, 759.

RENEWABLE HYDROGEN PRODUCTION BY CATALYTIC STEAM REFORMING OF PEANUT SHELLS PYROLYSIS PRODUCTS

Robert J. Evans¹, Esteban Chornet¹, Stefan Czernik¹, Calvin Feik¹, Richard French¹, Steven Phillips¹, Yaw D. Yeboah², Danny Day³, Shivayam Ellis³, Dennis McGee⁴, and Matthew J. Realf⁵

¹National Renewable Energy Laboratory,
1617 Cole Blvd, Golden, CO 80401

²Clark Atlanta University
Atlanta Ga 30314
M

³Scientific Carbons Inc
Blakely GA 31723

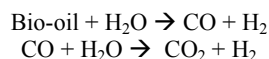
⁴Enviro-Tech Enterprises Inc
Matthews NC 28105

⁵Georgia Institute of Technology
Atlanta GA 30332

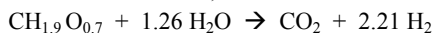
Introduction

The goal of this work is the production of renewable hydrogen from agricultural residues, in the near-term time frame and at a comparable cost to existing methane-reforming technologies. Near term production of renewable hydrogen from biomass requires a co-product strategy to compete with conventional production of hydrogen from the steam reforming of natural gas.^{1,2} The production of hydrogen by the processing of pyrolysis products that are produced as a by-product of activated carbon is one path that is possible to demonstrate the co-product strategy.

The original concept was that the pyrolysis oil could be fractionated into two fractions based on water solubility. The water-soluble fraction is to be used for hydrogen production and the water insoluble fraction could be used in adhesive formulations.³ The bio-oil can be stored and shipped to a centralized facility where it is converted to hydrogen via catalytic steam reforming and shift conversion. Catalytic steam reforming of Bio-oil at 750-850°C over a nickel-based catalyst is a two-step process that includes the shift reaction:



The overall stoichiometry gives a maximum yield of 17.2 g H/100 g bio-oil (11.2 wt.% based on wood):



The process has been demonstrated at the bench scale using model compounds and the carbohydrate-derived fraction of bio-oil.^{1,4} Regional networks of pyrolysis plants could be established to provide oil to a central steam reforming facility. The process is adaptable to other organic waste streams such as aqueous-steam fractionation processes used for ethanol production and trap grease. Recent laboratory work has demonstrated the feedstock flexibility with the processing of pyrolysis oil fractions from different feedstocks as well as other biomass-derived streams such as glycerine from biodiesel production, trap grease, and wood hydrolysis effluents.⁵

Although the adhesive byproduct option remains viable, commercial deployment opportunities are still not near term. Hence, other opportunities had to be developed based on the co-product strategy. The conversion of biomass to activated carbon is an alternative route to hydrogen with a valuable co-product as outlined in Figure 1. Slow pyrolysis is used in the first step of the activated

carbon process to optimize the yield of charcoal and organic vapors. Southwest Georgia was identified as an excellent opportunity because of the importance of agriculture, the forest product industry, and the need for zero emission transportation fuels in the Atlanta area. Scientific Carbons Inc. in Blakely GA uses pelletized peanut shells as the feed material for the production of activated carbon. They feed the densified peanut shells to a two-stage process producing activated carbon. The vapor by-products from the first stage, pyrolysis, are currently used as fuel for steam generator.

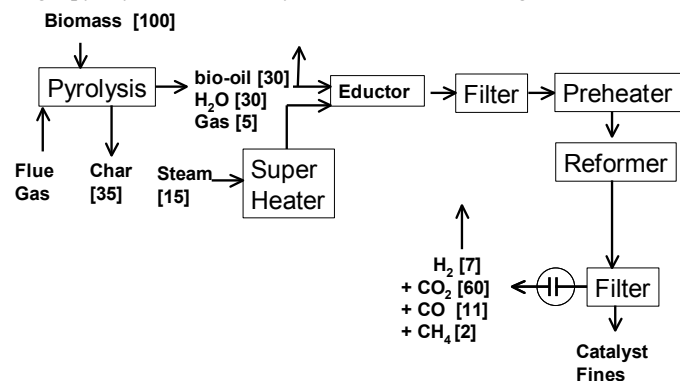


Figure 1. Mass Balance and Unit Operations in the Pyrolysis of Biomass to Activated Carbon and Steam Reforming of vapors to Hydrogen

Work at the bench scale at NREL has is promising with run times in a two-inch fluid bed reactor of over 100 hours. Systematic studies of variation in catalyst composition have shown that commercial steam reforming catalysts perform optimally for the conversion.⁶ However, physical attrition is a problem since these catalysts are not manufactured for fluid bed operation.⁴

This paper reports on the first performance of the scaled-up catalytic steam-reforming reactor and on the initial tests for conversion of whole biomass pyrolysis vapors to hydrogen.

Experimental

Pelletized peanut shells were fed to a cross-draft, moving-bed pyrolysis reactor heated by propane combustion gases. Superheated steam was used to educt a fraction of the vapors through a bag house to remove char fines and then to a preheater before the reformer. 50 kg/hour of pelletized peanut shells were fed to the pyrolysis reactor that was controlled so the exit gas temperature was 500 °C. Using a helium tracer it was determined that 20% of the gaseous products were educted in the steam flow to the reformer. The steam/vapor stream then enters a preheater that raises its temperature to 650-700°C.

The catalytic fluid bed reformer was fed 5 kg/h of pyrolysis vapor. The maximum allowable operating temperature and pressure are 900 °C and 140 kPa, respectively. The reformer is equipped with internal and external cyclones for disengaging catalyst particles, instrumentation, data acquisition, and safety features (alarms, etc.). Commercial nickel-based catalyst grounded to particle size of 300-500 μ is being used in the reactor. The catalyst is fluidized using superheated steam, which is also a reactant in the reforming process. The cyclones capture both fine catalyst particles and solid carbon generated by gas phase pyrolysis of the vapors that may occur in competition with the catalytic steam reforming. The Inconel reactor with a porous material distribution plate is placed inside a three zone electric furnace to maintain the reactor at the desired temperature during the endothermic steam reforming operation. The reformed

products flow through the spray scrubbers and a cold wall condenser before passing through a coalescing filter to remove aerosols.

Results and Discussion

The purpose of the run was to reform the whole pyrolysis vapors (for the first time) in the 5 cm catalytic steam reforming fluid bed reactor. The more chemically stable, lignin-derived phenolics may be more likely to coke on the nickel catalyst. Prior runs in the 5 cm reformer have used only the aqueous carbohydrate-derived fraction of pyrolysis oil.

Gas composition at the outlet of the reformer was monitored during the operation and is shown in Figure 2. The composition of the gas indicates that the yield of hydrogen from this agricultural residue feedstock is approximately 90% of maximum. Additional optimization of process conditions should result in somewhat higher yields (note that, in a commercial operation, the remaining CO would be converted to additional hydrogen using conventional water-gas shift processing). Initial performance was variable due to unstable conditions in the reformer. A period of stable operations was then achieved until a pressure drop across the hot gas filter led to unstable operation. In these tests, the gas product stream was flared. No breakthrough of pyrolysis products was noted and the methane level, which is a sensitive indicator of catalyst activity, did not increase. The significant finding here is that the lignin-derived pyrolysis products were reformed completely. The changes in product gases were due to a systematic decrease in mass flow to the bed due to an increase in pressure drop across the hot gas filter. This build up of particulates was unexpected, but the change in product gas composition indicates better performance with an increase in hydrogen yield and decrease in relative yield of both CO and CH₄ by effectively decreasing the weight hourly space velocity and increasing the steam to carbon ratio, we achieved a higher rate of conversion most likely by allowing more time for carbon gasification from the catalyst surface.

Summary and Future Work

The steam reforming of biomass pyrolysis oil, when integrated with the production of high value products, is a promising near-term approach to the production of renewable hydrogen. The application in Georgia is at a plant that makes activated carbon from peanut shells and has pyrolysis by-products available for conversion. The key technical goals for the run are to obtain preliminary performance data on the catalyst, especially physical attrition and deactivation.

In the next phase, the reactor will be run for 1000 hours with additional gas stream processing included. The hydrogen that is produced will be purified by separating hydrogen from CO and CO₂ using pressure swing adsorption. The purified hydrogen will be mixed with natural gas and used in engine demonstrations. Other agricultural residues and deployment logistics are being evaluated for cost and co-product potential.^{7,8}

The hydrogen produced in the next phase of the project will be blended with CNG and used in a transportation demo. This integrated strategy will demonstrate the potential impact of hydrogen and bioenergy on the economic development and diversification of rural areas.

Acknowledgement. The authors gratefully acknowledge the support of the DOE Hydrogen Program

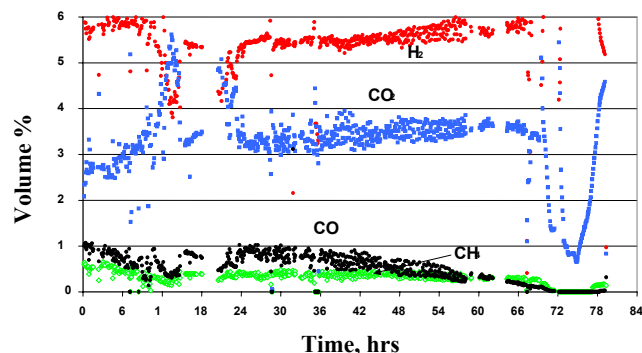


Figure 2. Gas composition from reforming peanut-shell pyrolysis vapors

References

1. Chornet, E.; Czernik, S.; Wang, D.; Gregoire, C.; Mann, M., In *Proceedings of the 1994 DOE/NREL Hydrogen Program Review*, Livermore, California, NREL/CP-470-6431; CONF-9404194, **1994**, pp. 407-432.
2. Spath, P.L.; Mann, M.K., In *Hydrogen Energy Progress XII. Proceedings of the 12th World Hydrogen Energy Conference*, Buenos Aires, Argentina, Bolcich, J. C. and Veziroglu, T. N., Eds. Vol. 3, **1998**, pp. 2057-2067.
3. Kelley, S.S.; Wang, X.-M.; Myers, M. D.; Johnson, D. K.; Scahill, J. W., In *Developments in Thermochemical Biomass Conversion*, Bridgwater, A. V. and Boocock, D. G. B., Eds., London: Blackie Academic & Professional, **1997**, pp. 557-572.
4. Chornet, E.; Czernik, S.; Feik, C.; French, R., In *Proceedings of the 2001 DOE/NREL Hydrogen Program Review*, Baltimore, MD., **2001**.
5. Czernik, S., French, R.; Feik, C.; Chornet, E., In *Progress in Thermochemical Biomass Conversion*, Bridgwater, A. V., Ed. London: Blackwell Science Ltd., **2001**, pp. 1577-1585.
6. Garcia, L., French, R.; Czernik, S.; Chornet, E., *Applied Catalysis A: General*, **2000**, *201*, 225-239.
7. Abedi, J.; Yeboah, Y. D.; Realf, M.; McGee, D.; Howard, J.; Bota, K.B. In *Proceedings of the 2001 DOE/NREL Hydrogen Program Review*, Baltimore, MD., **2001**.
8. Ozyurt, B. D., Realf, M. J., In *AIChE National Meeting Special Symposium*, Dallas, TX., **1999**.

Steam Gasification of Cellulose by Continuous Cross-Flow Moving Bed Type Differential Reactor

Yohsuke Yamaguchi, Chihiro Fushimi, Takeshi Furusawa
Atsushi Tsutsumi

Department of Chemical System Engineering
The University of Tokyo
7-3-1 Hongo, Bunkyo-ku, Tokyo 113-8656 Japan

Introduction

Steam gasification is a promising technology for thermochemical hydrogen production from biomass. However, a large amount of tar is produced in the biomass gasification process. This reduces thermal efficiency and causes tar troubles such as pipeline plugging and defluidization. Thus, it is very important to investigate the reaction mechanism of tar production in gasification for improvement in controllability and thermal efficiency of biomass gasifiers.

Several researchers have investigated the products and reaction mechanism of cellulose pyrolysis.¹⁻⁶ The generally accepted mechanism for cellulose pyrolysis (Broid-Shafinzadeh model¹) consists of three coupled first order steps. There is an initial step, involving no weight loss that leads to activated cellulose the nature of which is not well understood. This is followed by a pair of competing reactions, which produces either volatiles or char and gases. Both of the two reactions lead to weight loss.¹⁻⁴ Antal *et al.* reported that the presence of steam in the pyrolysis medium had no measurable effect on cellulose pyrolysis kinetics.⁷

In the conventional methods, it is impossible to investigate the time profile of tar production in steam gasification of biomass with rapid heating in continuous feeding condition. Thus, in this study, we have developed a continuous cross-flow moving bed type differential reactor and investigated the time profile of tar evolution and char production in gasification of biomass.

Experimental

Figure 1 shows the schematic diagram of experimental apparatus. Sample was continuously fed into a preheated quartz glass reactor and conveyed by a belt through the reactor. The reactor was divided into six compartments (W90 mm×D80 mm×H40 mm) whose gas flows were independent. Steam was fed with Ar carrier gas. Gas and tar can be collected separately in accordance with the evolving time. Char was collected at the end of the reactor.

Cellulose (< 160 μm), which is major component of biomass, was used as a sample. The gaseous products (H₂, CO, CO₂, CH₄, C₂H₄ and C₂H₆) were analyzed by a micro GC. The compositions of tar and char were analyzed by a Total Organic Carbon (TOC) analyzer, a CHNS elemental analyzer and FT-IR. Molecular weight of tar was also analyzed by a Gel Filtration Chromatograph (GFC). The experiments were carried out at 673 K

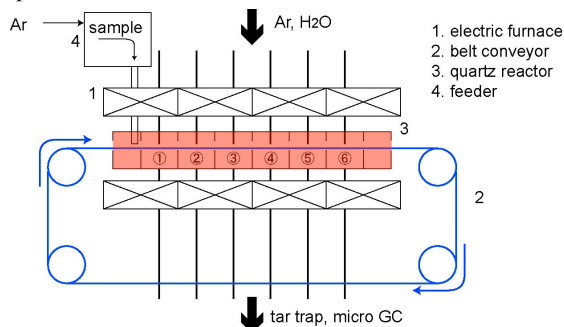


Figure 1. Schematic diagram of experimental apparatus

Results and Discussion

Analysis of gas and tar. Figure 2 shows time profile of gas evolution rate and temperature of each compartment. The initial time (0 s) was defined as the sample was fed into the reactor. The X-axis represents the time when the sample went through the middle point of the each compartment. Evolution of CO₂ and CO was dominant and that of other gases was negligible at this temperature. It is considered that CO₂ production was dominant because of the equilibrium of water-gas-shift reaction. The major product was tar at this temperature (not shown).

Table 1 shows elemental composition of produced tar. The amount of oxygen was calculated by difference. The elemental composition of tar was quite similar to that of original cellulose. Figure 3 shows the molecular weight distribution of tar measured by GFC. The components with lower molecular weight are detected with increasing retention time. The molecular weight of the three peaks was 210, 326 and 486. Since the molecular weight of unit cellulose (C₆H₁₀O₅) is 162, the three peaks can be assigned to monomer (levoglucosan), dimer (cellobiosan) and trimer (cellotriosan) of cellulose. It was found that evolved tar in steam gasification was cellulose with low degree of polymerization and that the major components are levoglucosan and cellobiosan.

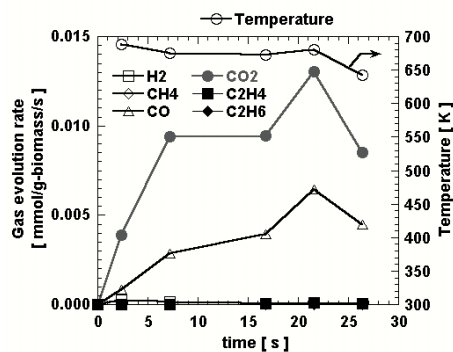


Figure 2. Time profile of gas evolution

Table 1. Elemental composition of produced tar

time [s]	C	H	O (diff.)
0 (cellulose)	44.4	6.2	49.4
2.4	45.3	5.5	48.4
7.2	46.8	5.1	47.4
16.8	48.8	5.8	44.7
21.6	47.8	5.9	45.6
26.4	47.2	5.9	46.1

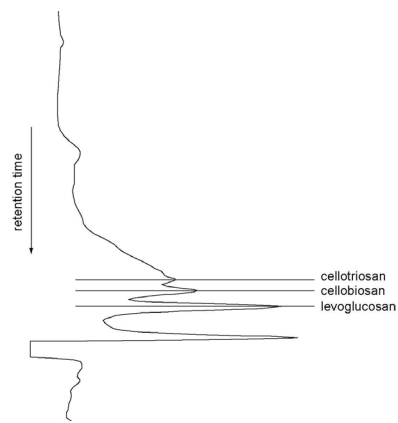


Figure 4. Molecular weight distribution of tar

Analysis of char. Char was collected by changing velocity of the belt (residence time=14.4, 28.8, 57.6 and 115.2 s) and analyzed. **Figure 4** shows time profile of conversion to volatile matter calculated from the weight reduction of char. It can be seen that the weight reduction of cellulose started about 20 s and was completed in 57.6 s. **Table 2** shows the elemental composition of char. It can be seen from this table that the elemental composition of char was quite similar to that of cellulose until 57.6 s. However, the elemental composition of char was significantly changed at 115.2 s although the weight of char was not changed in this period. In order to investigate the reaction in this period, the atomic ratios H/C and O/C were calculated and plotted on Krevelen's coal band (**Figure 5**). It was found that dehydration of char occurs after volatile release is completed. **Figure 6** shows FT-IR spectra. It was observed that the spectra of char were similar to that of cellulose up to 57.6 s. However, the peak at $3400\text{--}3000\text{ cm}^{-1}$ (OH groups) was weaker and those of 1700 cm^{-1} (C=O bond) and 1600 cm^{-1} (C=C bond) were stronger at 115.2 s. This also indicates the occurrence of dehydration of char.

Figure 7 shows reaction mechanism of steam gasification of cellulose. When cellulose is heated, at first depolymerization of cellulose takes place. Then evolution of tar with low degree of polymerization takes place. The major components of tar are levoglucosan and cellobiosan. After the tar evolution is completed, dehydration of char takes place.

Conclusions

Steam gasification of cellulose was studied using a continuous cross-flow moving bed type differential reactor. The following conclusions are drawn.

- (1) Depolymerization of cellulose takes place before volatiles are evolved. This does not lead weight decrease in the initial stage of gasification.
- (2) The evolved tar is cellulose with low degree of polymerization. Most of them are levoglucosan and cellobiosan.
- (3) Dehydration of cellulose char occurs after the evolution of tar is completed.

Acknowledgement. This study was financially supported by "Core Research for Evolutional Science and Technology" grant from Japan Science and Technology Corporation (JST). The authors appreciate this financial support.

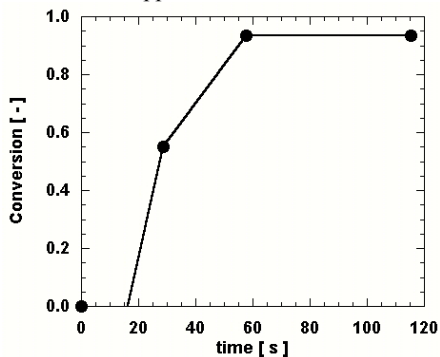


Figure 4. Time profile of conversion to volatile matter calculated from the weight of char

Table 2. Elemental composition of char

time [s]	C	H	O (diff.)
0 (cellulose)	44.4	6.2	49.4
14.4	44.7	6.2	48.2
28.8	45.5	6.2	47.5
57.6	46.6	6.0	46.7
115.2	64.5	4.0	30.9

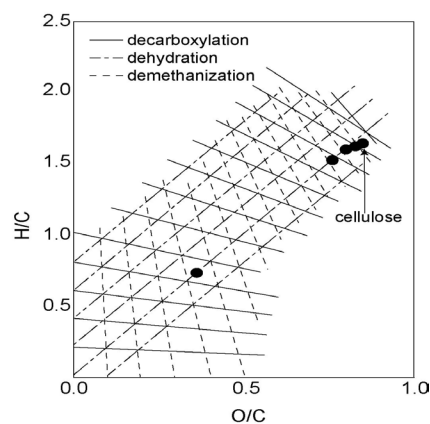


Figure 5. Krevelen's coal band

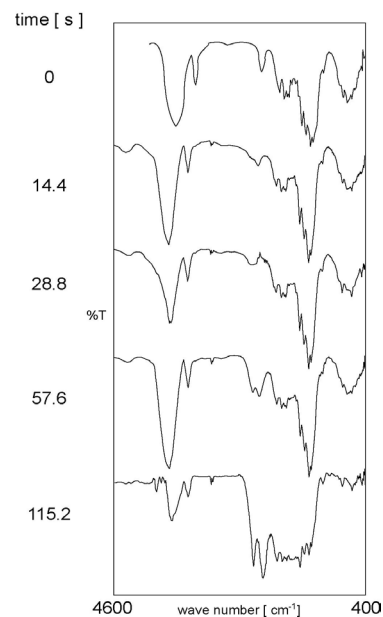


Figure 6. IR spectra of char

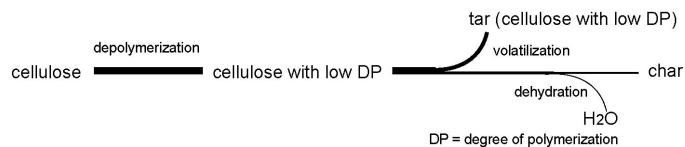


Figure 7. Reaction mechanism of steam gasification of cellulose

References

- (1) Bradbury, A. G. W.; Sakai, Y.; Shafizadeh, F. *J. Applied Polymer Science*, **1979**, *23*, 3271.
- (2) Banyasz, J. L.; Li, S.; Lyons-Hart, J.; Shafer, K. H. *J. Anal. Appl. Pyrolysis*, **2001**, *57*, 223.
- (3) Banyasz, J. L.; Li, S.; Lyons-Hart, J.; Shafer, K. H. *Fuel*, **2001**, *80*, 1757.
- (4) Li, S.; Lyons-Hart, J.; Banyasz, J.; Shafer, K. H. *Fuel*, **2001**, *80*, 1809.
- (5) Alves, S. S.; Figueiredo, J. L. *J. Anal. Appl. Pyrolysis*, **1989**, *17*, 37.
- (6) Pouwels, A. D.; Eijkel, G. B.; Boon, J. J. *J. Anal. Appl. Pyrolysis*, **1989**, *14*, 237.
- (7) Antal, M. J.; Friedman, H. L.; Robers, F. E. *Combustion Science Technology*, **1980**, *21*, 141.

Plasma Gasification of Biomass in a Downflow Reactor

Zengli Zhao Haibin Li Chuangzhi WU Yong Chen

(Guangzhou Institute of Energy Conversion, CAS, Guangzhou
510070)

Abstract : The experiments of biomass gasification have been carried out using a plasma reactor, which has high temperature and high enthalpy. The product includes solid char and gas. No tar was detected. Synthesis gas (H_2+CO) is the main gas product. With the steam flow increasing, H_2/CO molar ratio ranges from 0.90 to 1.15. The gas yield is about 2L per g of biomass and the combined volume of H_2 and CO was 96%. The gas conversion of carbon was very high.

Keywords: Biomass, Plasma, Gasification

FUEL FORMULATION EFFECTS ON DIESEL PARTICULATE FILTER REGENERATION

André Boehman, Juhun Song, Mahabubul Alam and Vince Zello

The Energy Institute
The Pennsylvania State University
405 Academic Activities Building
University Park, PA 16802

Kirk Miller

ConocoPhillips
600 N. Dairy Ashford
Houston, TX 77252

Introduction

Diesel particulate emissions pose a significant potential health hazard. Control of diesel particulate emissions is an issue requiring the attention of the fuels, engine and aftertreatment industries. To achieve the reductions in particulate emissions mandated by the US Environmental Protection Agency in 2007, use of diesel particulate filters (DPF) will be a necessity [1]. To enable the implementation of particulate and NO_x control technologies, the US EPA has mandated that ultra low sulfur fuels be available to enable advanced aftertreatment strategies, which can be highly sulfur sensitive [2]. A critical requirement for implementation of diesel particulate filters on diesel-powered vehicles is having a low “break even temperature,” defined as the temperature at which particulate deposition on the filter is balanced by particulate oxidation on the filter. This balance point needs to occur at sufficiently low temperatures to fit within the exhaust temperature range of a typical diesel vehicle duty cycle. Catalytic coating on the diesel particulate filter, use of a fuel borne catalyst and oxidation catalysts placed upstream of the particulate filter can all reduce this balance point temperature. Another important factor in lowering the balance point temperature is fuel sulfur content, because the sulfur dioxide generated during combustion can poison catalyst activity [1,2].

Modification of diesel fuel composition, for example, by blending with oxygenated fuels, can contribute to reducing emissions. Addition of biomass-derived fuels and synthetic fuels to diesel fuel basestocks is a means of producing a cleaner burning diesel fuel. Blending with oxygenated or zero sulfur fuels can lead to particulate emissions reductions by interfering with the soot formation process and by decreasing the formation of sulfates. However, in the case of biodiesel fueling (e.g., “B20”, a blend of 20vol.% methyl soyate in diesel fuel) there is a well documented increase of 2-4% in NO_x emissions [3]. As shown by Van Gerpen and co-workers [4,5] and Szybist, et al. [6], the NO_x increase with biodiesel fueling is attributable to an inadvertent advance of fuel injection timing. The advance in injection timing is due to the higher bulk modulus of compressibility, or speed of sound, in the fuel blend, which leads to a more rapid transfer of the pressure wave from the fuel pump to the injector needle and an earlier needle lift.

In this paper we present comparative study of the impact of sulfur content and biodiesel blending on particulate trap operation. The means of comparison is analysis of the impact of fuel composition on the break even temperature.

Experimental

Tests were performed with a Cummins ISB 5.9L turbodiesel engine (MY2000, 235 HP max output) connected to a 250 HP capacity, eddy current absorbing dynamometer. The engine has been heavily instrumented, with a 0.1 crank angle resolution crank shaft

encoder, a cylinder pressure sensor, a needle lift sensor and in-cylinder visualization using an AVL 513D Engine Videoscope. The engine and dynamometer are operated through an automated control system. Connected to the engine exhaust is a catalyzed diesel particulate filter. Exhaust samples are pulled upstream and downstream of the DPF, while exhaust temperature, filter temperature and pressure drop across the DPF are monitored.

Test Procedure. Prior to a break even temperature (BET) test, the filter is cleaned of particulate via operation at elevated temperature. Then, the exhaust temperature is reduced while the filter is filled with particulate matter until the pressure drop across the filter reaches 20 inches of H₂O. Then, exhaust temperature is increased in steps by increasing the load on the engine. Four fuel formulations were considered, a low sulfur diesel fuel (LSD, 325 ppm sulfur), ultra low sulfur diesel fuel (ULSD, 15 ppm sulfur), a 20 vol.% blend of biodiesel (“B20”) with LSD (LSD/B20) and a B20 blend with ULSD (ULSD/B20).

Particulate mass measurements are obtained with a Sierra Instruments BG-1 Micro Dilution Test Stand by sampling onto Pallflex 90 mm filters. Measurement of the soluble organic fraction (SOF) of the particulate matter is performed by weighing the sample filter before and after solvent extraction using dichloromethane (DCM). Gaseous emissions were obtained with an AVL CEB II raw diesel emissions bench.

Results and Discussion

As shown recently by Szybist and Boehman [7], fuel injection timing advances of 0.3 crank angle (CA degrees) and 1 CA degree are observed in “pump-line-nozzle” configuration fuel systems, for B20 and B100 respectively. This injection timing advance in a purely mechanical fuel injection system may not be as likely in an electronically controlled fuel injection system. In the Cummins ISB engine, the Bosch fuel system is electronically controlled which potentially complicates the interpretation of fuel effects on injection timing. The engine controller itself may shift injection timing due to differences in throttle position required to meet the required load because of differences in the calorific value of the test fuels.

Figure 1 shows the particulate composition during the filter loading period and indicates that there are some modest differences in the rate and composition of the particulate that is depositing on the DPF.

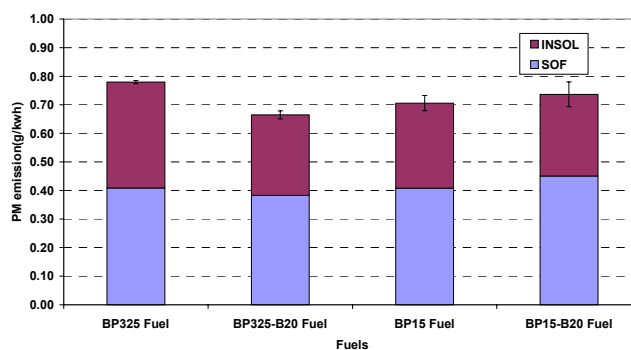


Figure 1. Particulate composition during the filter loading process for the various test fuels.

Figure 2 shows the variation of engine-out NO_x emissions during the filter regeneration process, caused by the differences in fuel composition and the presence of biodiesel fuel. Figure 3 shows the extent of conversion of engine-out NO to NO₂ across the

catalyzed DPF due to oxidation. Figure 4 indicates the variation in break even temperature with test fuel composition. The BET is determined by following the slope in the variation of pressure drop as exhaust temperature increases.

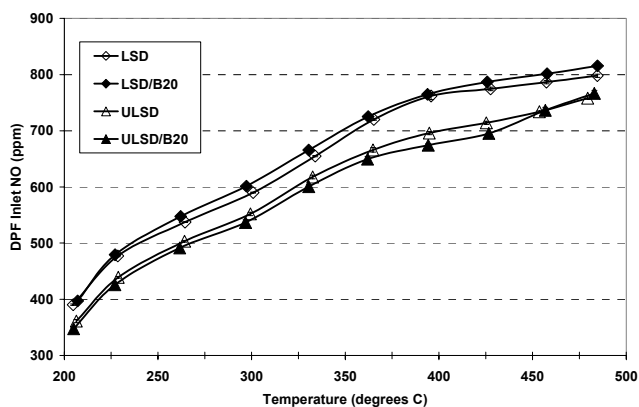


Figure 2. Variation in engine-out NOx emissions during the filter regeneration process for the various test fuels.

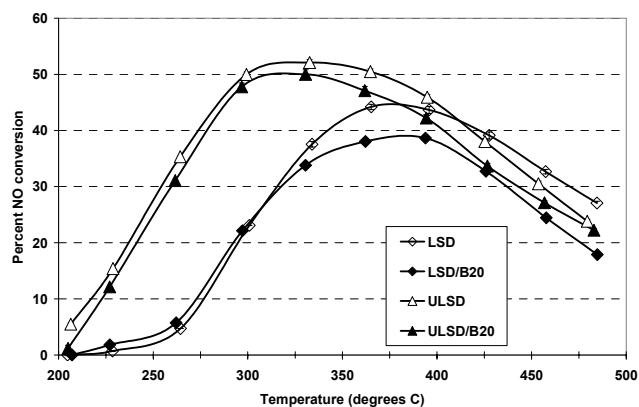


Figure 3. Variation in NO conversion to NOx across the DPF during the filter regeneration process for the various test fuels.

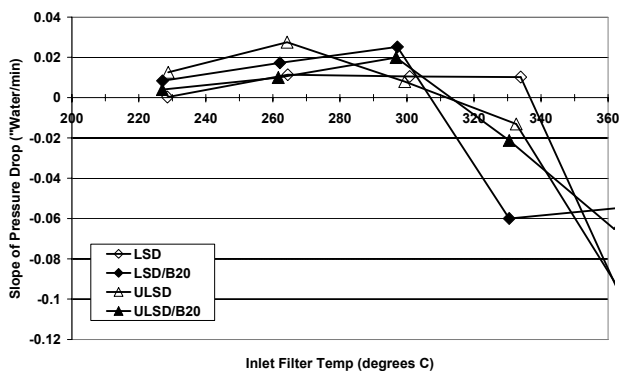


Figure 4. Filter temperature versus slope of the pressure drop, indicating the break even temperature for the various test fuels.

The results in Figures 1-4 show that although there is modest variation in the composition and mass emissions rate of particulate matter from the engine between the test fuels, there are differences in engine-out NOx and, as a consequence, NO conversion across the catalyzed DPF. For both base fuels, the LSD and ULSD, there is an engine-out increase in NOx, which is comprised mostly of NO. Subsequently, the engine-out NO is oxidized to NO₂ over the catalyst that is impregnated into the DPF. The NO₂ assists in the oxidation of the particulate matter on the DPF, because NO₂ is a more aggressive oxidizer of diesel particulate matter than O₂ [1]. However, the conversion of NO to NO₂ is inhibited by the presence of SO₂ in the exhaust, which is 20 times higher for the LSD than for the ULSD. So, the NO conversion to NO₂ is lower and requires an additional 100°C exhaust temperature to become significant for the LSD due to its higher sulfur content.

Of great interest is that the net effect of the higher engine-out NOx emissions for the LSD/B20 fuel leads to the lowest break even temperature, 308°C. Consistent with one's expectations, the LSD has the highest BET. However, the ULSD and ULSD/B20 fuels yield the same BET. This difference in BET may be explained by the generally lower NOx emissions for the ULSD and ULSD/B20 fuels relative to the LSD and LSD/B20 fuels. There is more NOx with the LSD and LSD/B20 fuels to serve to oxidize the particulate matter on the DPF after conversion of NO to NO₂, but for the LSD the NO conversion is inhibited and the particulate oxidation is inhibited by the higher sulfur content.

Conclusions

While there is ample evidence in the literature of the deleterious effects of sulfur on aftertreatment devices, the results presented here show that other fuel related phenomena can have just as significant an effect on the performance of an aftertreatment device. In this specific case, the lowest break even temperature for a catalyzed DPF was observed with biodiesel blended into a low sulfur fuel.

Acknowledgement The authors wish to thank ConocoPhillips for its support of this work and Keith Lawson and Etop Esen of ConocoPhillips for their technical guidance.

This paper was written with support of the U.S. Department of Energy under Cooperative Agreement No. DE-FC26-01NT41098. The Government reserves for itself and others acting on its behalf a royalty-free, nonexclusive, irrevocable, worldwide license for Governmental purposes to publish, distribute, translate, duplicate, exhibit, and perform this copyrighted paper.

References

- (1) Allansson, R., et al., "Optimising the Low Temperature Performance and Regeneration Efficiency of the Continuously Regenerating Diesel Particulate Filter (CR-DPF) System," SAE paper 2002-01-0428, 2002.
- (2) Schmidt, D., et al., "Review and assessment of fuel effects and research needs in clean diesel technology," ASME ICE-Vol 36-1, 2001, p. 23-36.
- (3) Graboski, M.S. and R.L. McCormick, "Combustion of fat and vegetable oil derived fuels in diesel engines." *Progress in Energy and Combustion Science*, 1998, **24**(2): p. 125-164.
- (4) Monyem, A., J.H. Van Gerpen, and M. Canakci, "The effect of timing and oxidation on emissions from biodiesel- fueled engines". *Transactions of the ASAE*, 2001, **44**(1): p. 35-42.
- (5) Tat, M.E., et al., "The speed of sound and isentropic bulk modulus of biodiesel at 21 degrees C from atmospheric pressure to 35 MPa." *Journal of the American Oil Chemists Society*, 2000, **77**(3): p. 285-289.
- (6) Szybist, J.P., et al., "Diesel fuel formulation effects on injection timing and emissions," Prepr. Pap. - *Am. Chem. Soc., Div. Fuel Chem.*, **2003**, **48**(1), 428.
- (7) Szybist, J.P. and A.L. Boehman, "Behavior of a diesel injection system with biodiesel fuel," Society of Automotive Engineers Technical Paper No. 2003-01-1039, 2003.

BIODIESEL PRODUCTION BY A CONTINUOUS PROCESS USING A HETEROGENEOUS CATALYST.

Gerard Hillion ⁽¹⁾, Bruno Delfort ⁽¹⁾, Dominique le Pennec ⁽¹⁾,
Laurent Bournay ⁽¹⁾, Jean-Alain Chodorge ⁽²⁾

⁽¹⁾ Institut Français du Pétrole (IFP), 1&4 av de Bois Préau, 92852
Rueil-Malmaison Cedex - France

⁽²⁾ Axens, IFP Group Technologies, 89 bd F. Roosevelt, 92508 Rueil-
Malmaison Cedex - France

Introduction

The reactions for direct transformation of vegetable oils into methyl esters and glycerol have been known for more than a century. The reactions of interest today, mainly those producing methyl esters from rapeseed, soybean and sunflower oils, have been studied and optimized in order to manufacture the high quality diesel fuel known as biodiesel.

With over ten years of development and commercial use in Europe, biodiesel has now proved its value as a fuel for diesel engines [1-3]. The product is free of sulfur and aromatics, and, as it is obtained from renewable sources, it reduces the lifecycle of carbon dioxide emissions by almost 70% compared to conventional diesel fuel. Moreover, recent European regulations have restricted sulfur content in diesel fuel to no more than 50 ppm in year 2005. Sulfur is known to provide diesel fuels with a lubricity that will disappear as the regulations take effect. Biodiesel addition at levels of one to two per cent in diesel blends has the beneficial impact of restoring lubricity through an antiwear action on engine injection systems [4-5].

Several commercial processes to produce fatty acid methyl esters from vegetable oils have been developed and are available today. These processes consume basic catalysts such as caustic soda or sodium methylate which form unrecyclable waste products. This paper provides a general description of a new process using a heterogeneous catalytic system.

Biodiesel Production Processes

The transesterification of triglycerides to methyl esters with methanol is a balanced and catalyzed reaction as illustrated in Figure 1. An excess of methanol is required to obtain a high degree of conversion.

Rapeseed and soybean oils are among the main vegetable oil candidates for biodiesel uses. Their compositions are summarized in Table 1.

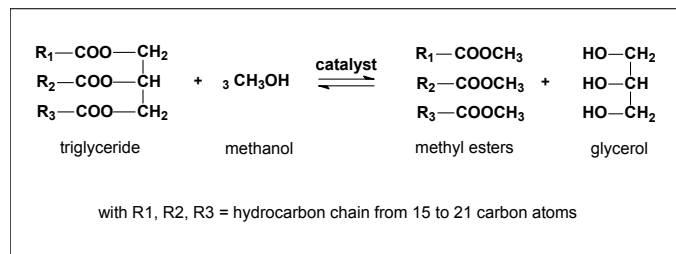


Figure 1. Overall reactions for vegetable oil methanolysis

The conventional catalysts in natural oil transesterification processes are selected among bases such as alkaline or alkaline earth hydroxides or alkoxides [6]. However, transesterification could also be performed using acid catalysts, such as hydrochloric, sulfuric and

sulfonic acid, or using metallic base catalysts such as titanium alcoholates or oxides of tin, magnesium, or zinc. All these catalysts act as homogeneous catalysts and need to be removed from the products after the methanolysis step.

Table 1. Fatty Acid Compositions for Rapeseed Oil and Soya Oil (weight %)

Fatty Acid Chain		Rapeseed Oil	Soybean Oil
Palmitic	C16:0	5	10
Palmitoleic	C16:1	< 0.5	
Stearic	C18:0	2	4
Oleic	C18:1	59	23
Linoleic	C18:2	21	53
Linolenic	C18:3	9	8
Arachidic	C20:0	< 0.5	< 0.5
Gadoleic	C20:1	1	< 0.5
Behenic	C22:0	< 0.5	< 0.5
Erucic	C22:1	< 1	

Conventional Homogeneous Catalyzed Processes. In conventional industrial biodiesel processes, the methanol transesterification of vegetable oils is achieved using a homogeneous catalyst system operated in either batch or continuous mode.

In most cases the catalyst is sodium hydroxide or sodium methylate. It is recovered after the transesterification reaction as sodium glycerate, sodium methylate and sodium soaps in the glycerol phase. An acidic neutralization step with, for example, aqueous hydrochloric acid is required to neutralize these salts. In that case glycerol is obtained as an aqueous solution containing sodium chloride. Depending on the process, the final glycerol purity is about 80% to 95%.

When sodium hydroxide is used as catalyst, side reactions forming sodium soaps generally occur. This type of reaction is also observed when sodium methylate is employed and traces of water are present. The sodium soaps are soluble in the glycerol phase and must be isolated after neutralization by decantation as fatty acids. The loss of esters converted to fatty acids can reach as high as 1% of the biodiesel production. These operations are illustrated in Figure 2.

Heterogeneous Catalyzed Process. To avoid catalyst removal operations and soap formation, much effort has been expended on the search for solid acid or basic catalysts that could be used in a heterogeneous catalyzed process [7-10]. Some solid metal oxides such as those of tin, magnesium, and zinc are known catalysts but they actually act according to a homogeneous mechanism and end up as metal soaps or metal glycerates.

In this paper a new continuous process is described, where the transesterification reaction is promoted by a completely heterogeneous catalyst. This catalyst consists of a mixed oxide of zinc and aluminium which promotes the transesterification reaction without catalyst loss. The reaction is performed at a higher temperature than homogeneous catalysis processes, with an excess of methanol. This excess is removed by vaporization and recycled to the process with fresh methanol.

The desired chemical conversion is reached with two successive stages of reaction and glycerol separation to displace the equilibrium reaction. The flow sheet for this process appears in Figure 3.

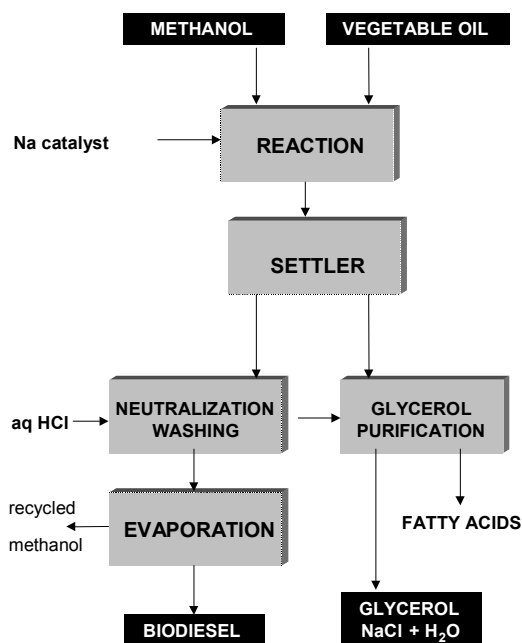


Figure 2. Global scheme for a typical continuous homogeneous catalyzed process.

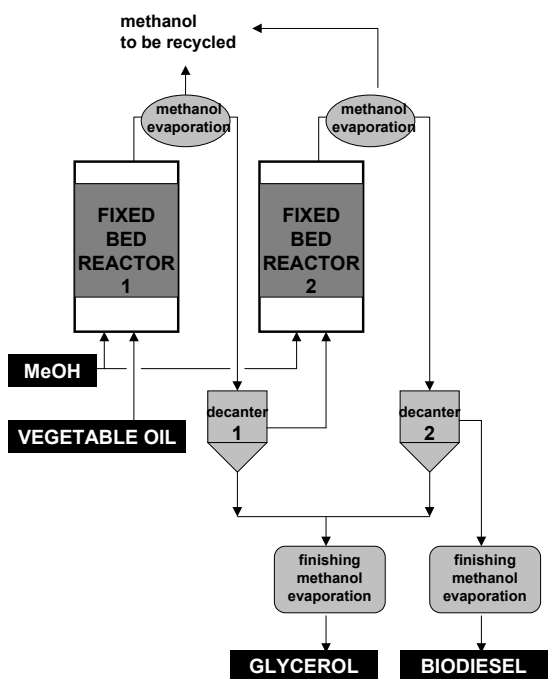


Figure 3. General scheme for a continuous heterogeneous catalyzed process

The catalyst section includes two fixed bed reactors that are fed by oil and methanol at a given ratio. Excess methanol is removed after each of the two reactors by a partial flash. Esters and glycerol are then separated in a settler. Glycerol phases are joined and the last traces of methanol are removed by vaporization. Biodiesel is

recovered after final recovery of methanol by vaporization under vacuum and then purified to remove the last traces of glycerol. Typical characteristics of biodiesel obtained from rapeseed oil and soybean oil in pilot plant operations are reported in Table 2.

Table 2. Main Characteristics of the Biodiesel Fuels Obtained from Rapeseed Oil and Soybean Oil with Heterogeneous Catalyzed Process.

Characteristics of Biodiesel		From Rapeseed Oil	From Soybean Oil	Required European Specifications
Methyl esters	wt - %	> 99.0	> 99.0	96.5
Monoglycerides	wt - %	0.5	0.5	0.8
Diglycerides	wt - %	0.02	0.02	0.2
Triglycerides	wt - %	0.01	0.01	0.2
Free glycerol	wt - %	< 0.02	< 0.02	0.02
Total glycerol	wt - %	0.15	0.15	0.25
Acid number	mg KOH /kg	< 0.3	< 0.3	0.5 max
Water content	mg/kg	200	200	500 max
Metal content	mg/kg	< 3	< 3	-
Phosphorus	mg/kg	< 10	< 10	< 10

General conditions : methanol/vegetable oil ratio : 1; temperature : 200°C; LHSV : 0.5h⁻¹

In this heterogeneous process, the catalyst is very stable with no metal leaching. There is no formation of either glycerate salts or metal soaps which affords the following advantages : no neutralization step is required, there is no introduction of water, and there is no salt formation; this accounts for an exceptional glycerol purity. In addition, there is no waste production of low-value fatty acids.

The purity of methyl esters exceeds 99% with yields close to 100% of the theoretical. Glycerol treatment is much easier than in homogeneous catalyzed processes. A simple elimination of methanol by vaporization suffices and no chemicals are required. The glycerol produced is neutral, clear and exempt from any salt, with purities above 98%. This valuable product could be used in many chemical applications without further treatment. If required, pharmaceutical grade can easily be reached.

The process feeds are limited to vegetable oils and methanol and the only products are biodiesel and a high-purity glycerol that is free of water and salt. With all its features, the process can be considered as a green process.

Experiments on methanolysis with acid-containing vegetable oils have also been conducted with no special acid removal treatment of the raw material. Methanolysis of a blend of 5% oleic acid in rapeseed oil leads to an ester product composition compatible with biodiesel requirements. In that case, esterification and transesterification reactions occur simultaneously. Results are summarized Table 3.

Table 3. Compositions of Ester Phases Obtained from Two Successive Fixed Bed Reactors (weight %). Neutralized Or Acidic Oil.

Feedstock Composition			Reactor 1		Reactor 2	
Rapeseed Oil (wt %)	Oleic Acid (wt %)	Acid Index	Methyl Esters (wt %)	Acid Index	Methyl Esters (wt %)	Acid Index
100	0	< 1	94.5	0.15	99.0	0.15
95	5	11	86.8	2.1	98.3	0.4

General conditions : methanol/vegetable oil ratio : 1; temperature : 200°C; LHSV : 0.5h⁻¹

Conclusions

Increasing biodiesel consumption requires optimized production processes that are compatible with high production capacities and that feature simplified operations, high yields, and the absence of special chemical requirements and waste streams. The high quality of the glycerol by-product obtained is also a very important economic parameter. A heterogeneous catalyzed continuous process allows all these objectives to be attained.

References

1. Wilson, E.K., *Chemical & Engineering News*, **2002**, May 27,
2. Biodiesel - A Success Story, *Report of the International Energy Agency*, February **2002**.
3. Vermeersch, G., *Oléagineux. Corps gras. Lipides.*, **2001**, 8, pp.33.
4. Montagne, X., *2nd European Motor Biofuels Forum*, Graz, September **1996**.
5. G. Hillion, X. Montagne, P. Marchand, *Oléagineux. Corps gras. Lipides.*, **1999**, 6, pp.435.
6. Kreutzer, U., *J. Am. Oil. Chem. Soc.*, **1984**, 61, pp.343.
7. Stern, R.; Hillion, G.; Rouxel, J. J.; Leporq, S. US Patent 5,908,946 (**1999**)
8. Stern, R.; Hillion, G.; Rouxel, J. J. US Patent 6,147,196 (**2000**)
9. Vogel, R. F.; Rennard, R. J.; Tabacek, J. A. US patent 4,490,479 (**1984**)
10. Gelbard, G.; Brès, O.; Vielfaure-Joly, F. *J. Am. Oil. Chem. Soc.*, **1995**, 72, ppl

Eliminating the NO_x Emissions Increase Associated with Biodiesel

Elana Chapman, Mike Hile, Mike Pague, Juhun Song,
André Boehman

Department of Energy and Geo-Environmental Engineering
Pennsylvania State University

Abstract

Implementing greater biodiesel use is inhibited in part because of the observed increase in NO_x emissions as compared to conventional petroleum diesel fuel. A relation between the saturation of the fuel with NO_x emissions has been established in the literature. This research explored two approaches of achieving a more saturated biodiesel fuel and observing its effects on NO_x emissions blended as B20. The first option explored is blending of the biodiesel fuel with short-chained, saturated methyl esters. The second is the hydrogenation of soybean oil prior to transesterification. A 60% caprylic/40% capric blend was mixed with B100 as a means of increasing the fuel's saturation. Another fuel containing a high percentage of oleic acid methyl ester was observed as an ideal hydrogenated fuel. Emissions testing revealed expected percentage decreased NO_x levels for the caprylic/capric blend, but the high oleic "hydrogenated" blend revealed a smaller NO_x emissions decrease than was expected.

Introduction

Biodiesel is an alternative diesel fuel created by the conversion of oils, fats and fatty acids to methyl and ethyl esters via esterification processes [1]. A variety of vegetable oils, typically soybean oil in the United States, and animal fats provide the source of the triglyceride fats and oils [2]. Continuous feedstock growth and livestock production provide a constant supply of source material allowing biodiesel to be a renewable source of fuel, which can be created domestically.

Additionally, biodiesel is miscible with petroleum-based diesel and works in any diesel engine with little or no modifications as pure biodiesel or as a blend with any other diesel fuel. In fact, biodiesel contains a higher oxygen content resulting in a more complete combustion of the fuel. Moreover, it is a cleaner burning fuel and reduces most harmful emissions such as particulate matter, unburned hydrocarbons and carbon monoxide.

However, a few issues need to be resolved before biodiesel fuels can be a prominent alternative fuel. The economics of providing an appropriate source material and of producing an affordable final product to create acceptable biodiesel fuels must be feasible. Moreover, engine emissions using biodiesel fuels typically increase emissions of oxides of nitrogen [3].

One approach appears to be increasing the degree of saturation of the ester molecules contained in the biodiesel. This report will investigate two potential options that may be used to achieve a higher degree of saturation: hydrogenation of the biodiesel fuel and the blending of the biodiesel fuel with a saturated methyl ester. Also presented are the results of calculations and experiments that were performed as a means of establishing these approaches as viable options to reduce NO_x emissions.

Biodiesel Processing

Vegetable oils are generally water-insoluble and consist of one mole of glycerol and three of fatty acids. They are more commonly referred to as triglycerides. The fatty acids contained in the oil vary in the length of the carbon chains, as well as the number of unsaturated (double) bonds [4]. In order to be used as a diesel

substitute the vegetable oil triglycerides must be converted to methyl esters. This is accomplished through the process of transesterification [4].

Experimental

The intent of the project is to decrease the NO_x emissions from biodiesel combustion through the saturation of the biodiesel methyl esters, specifically methyl esters made from soybean oil.

Blending Approach. The first option to achieve a higher saturation level in biodiesel fuel is to add an appropriate amount of a saturated methyl ester to the biodiesel. This was determined based on research by McCormick and coworkers, who determined the relationship between NO_x emissions and iodine value, as shown in Figure 1[5]. Additionally, it has been found that increasing the degree of saturation, increasing the length of the hydrocarbon chain and decreasing the degree of branching all affect the freezing points of organic molecules directly producing poor cold flow properties of biodiesel fuels [1, 6, 7]. Therefore, a blend of 60% caprylic acid methyl ester and 40% capric acid methyl ester (the "additive"), donated by Stepan Company, was chosen so that its short hydrocarbon chain length would help offset the adverse effect of saturation on cold flow properties.

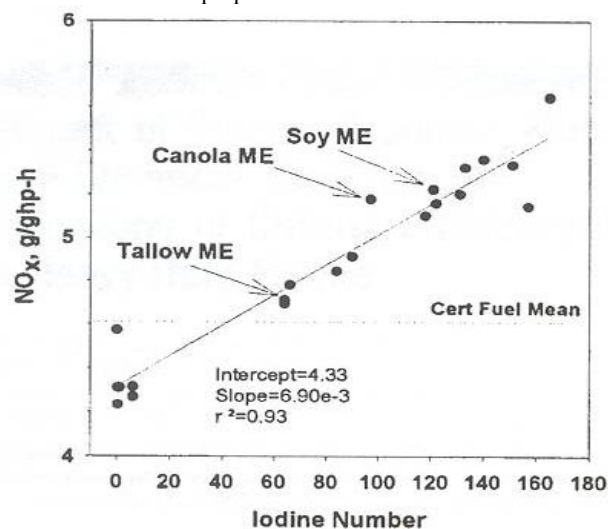


Figure 1. Iodine Number vs. NO_x [5].

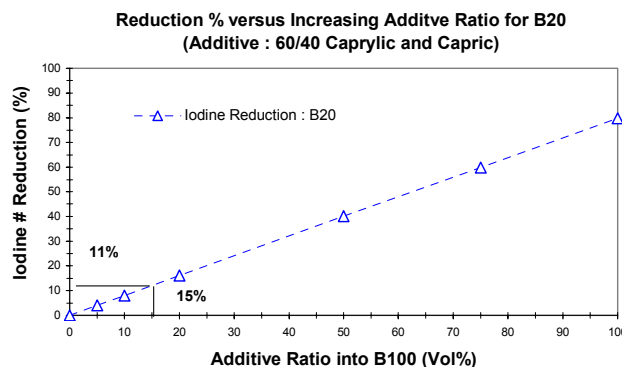


Figure 2. Reduction % versus increasing additive ratio for B20.

Hydrogenation Approach. The second option explored to this end was to use the industrial process of hydrogenation. Hydrogenation is, "the addition of hydrogen to a double or triple bond to yield a saturated product." [8] This option of saturation of

the molecules is particularly attractive as the process of hydrogenation is already being conducted on an industrial scale and is a well established technology. For this project, hydrogenated soy methyl ester was not available, so a substitute material was used which closely resembled the ideal iodine value, but did not adequately emulate the chemical composition.

Results and Discussion

It was observed that both options could reduce the NO_x emission by 1.5~3% relative to B20 fuel. Based on mode averaged NO_x reduction, caprylate/caprinate blending generated around 2.8 % NO_x reduction over all the modes that is expected as summarized in the right side of Figure 3, confirming that iodine and NO_x correlation holds still valid for B20 blends. The raw data is compared in Figure 4.

As hydrogenated B20 has a little lower iodine number and density than caprate added B20, it was expected that NO_x reduction of this will be greater than other if other properties change remains constant for NO_x. But this was less effective to reduce NO_x than blending as seen in the same plot.

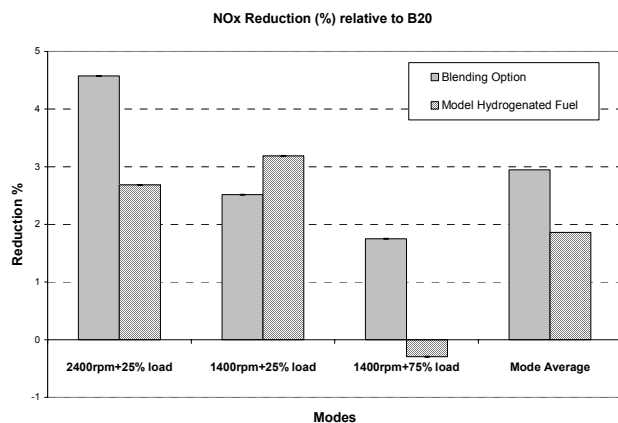


Figure 3. Percent NO_x emissions reduction relative to B20 blend.

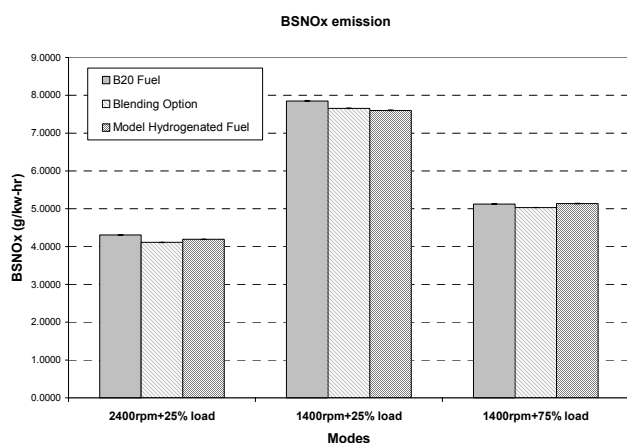


Figure 4. Brake specific NO_x emissions (BSNO_x) comparison.

Conclusions

From a review of literature, it was determined to focus the project investigation on the reduction of NO_x through the saturation of biodiesel methyl esters. Two approaches were taken to achieve this goal: blending and hydrogenation.

The blending approach involved the blending of short-chained, saturated methyl esters with biodiesel fuel. This approach was found to produce the desired reduction in NO_x emissions and improve the cold flow property. The NO_x reductions found in practice were in good agreement with predicted values. Unfortunately, while this option produced the desired results, the high cost of the saturated methyl esters makes this process economically unfeasible.

The second approach is the hydrogenation of soybean oil prior to transesterification. A second literature review was conducted to examine the process and process parameters of hydrogenation. Upon completion of this literature review, it was determined that hydrogenation is a viable option to increase the saturation of the biodiesel fuel methyl esters. To produce a blend that will reduce NO_x while not increasing the cloud point a high selectivity must be achieved during hydrogenation. Further research should be conducted to determine exact conditions for hydrogenation including temperature, catalyst type and loading, and pressure to produce the desired fatty acid chains. The experiments conducted on a fuel representing a hydrogenated product did show a reduction in NO_x emissions, but not to the extent predicted by calculations. This may be due to the fact that the fuel was lacking in stearic and palmitic acids. Another possible reason is that the engine used has an electronic controlled injection. This injection is very sensitive to fuel property such as heating value and density. As our "hydrogenated" fuel did not exactly match what a true hydrogenated biodiesel fuel would contain this test was not truly representative. If high selectivity is possible, hydrogenation is a viable solution to solve this problem as it is already in practice in the food industry.

Finally, increasing the saturation of biodiesel fuel is a way to reduce the emission of oxides of nitrogen. There are several methods to achieve this increase in saturation, two of which have been discussed here. Further research into hydrogenation or other methods of increasing saturation is suggested.

Acknowledgement. We would like to thank Dr. Robert McCormick of NREL, Dr. Michael Adewumi and Dr. André Boehman of Penn State, and Dr. Haas of the USDA Philadelphia Office. Additionally, we appreciate the support of P&G Chemicals and Stepan for their generous donation of the chemical supplies.

References

- Graboski, M.S., and McCormick, R.L., "Combustion of Fat and Vegetable Oil Derived Fuels in Diesel Engines." *Prog. Energy and Combust. Sci.*, 1998. **24**(2): p. 125-164.
- Suppes, G., Rui, Y., Regehr, E., "Hydrophilic Diesel Fuels- Ignition Delay Times of Several Different Fuel Blends." *Society of Automotive Engineers*, 1997 (971686).
- EPA, A Comprehensive Analysis of Biodiesel Impacts on Exhaust Emissions (EPA420-P-02-001). 2002, United States Environmental Protection Agency.
- Ma, F., Hanna, M., "Biodiesel production: a review." *Bioresources Technology*, 1999. **70**: p. 1-15.
- McCormick, R., Graboski, M., Alleman, T., Herring, A., Tyson, S., "Impact of Biodiesel Source Material and Chemical Structure on Emissions of Criteria Pollutants from a Heavy-Duty Engine." *Environ. Sci. Tech.*, 2001. **35**(9): p. 1742-1747.
- Gomez, M., Gonzalez, E., Howard-Hildige, R., Leahy, J., Rice, B., "Winterisation of Waste cooking oil methyl ester to improve cold temperatures fuel properties." *Fuel*, 2002. **81**(1): p. 33-39.
- Knothe, G., "Cetane number of branched and straight-chained fatty esters determined in an ignition quality tester." *Fuel*, 2002. **Article in Press**.
- McMurry, J., *Organic Chemistry*, 4th ed. 1995, Pacific Grove, CA: Brooks/Cole Publishing Company.

EFFECTS OF BIOMASS BLENDING ON COMBUSTION ASH

Christopher J. Zygarlicke and Bruce C. Folkedahl

Energy & Environmental Research Center (EERC)
University of North Dakota
Box 9018
Grand Forks, ND 58202-9018

Introduction

Cofiring biomass and coal in stoker-fired combustion systems may create some technical challenges. The diversity of the inorganic content of various biomass types coupled with the already known diversity of coal compositions makes it difficult to predict with great certainty the combustion performance of biomass-coal combinations. Recent work shows that intense characterization of biomass inorganics and controlled combustion experiments may aid in determining the behavior of combustion ash materials, including the interaction of biomass-derived alkali such as potassium with coal silicates. Mechanisms of ash deposit and fly ash particulate formation, including the role of fine silica, alkali, and alkaline-earth elements, and chlorine in biomass are being investigated (1–5). Stoker-fired boilers are popular for biomass cofiring because of the ease of fuel feeding, but even with these systems, issues such as production of different concentrations and quantities of fine particulate or aerosols, ash deposition rates, and the strength of ash deposits do arise. (6). In this paper, fundamental mechanisms of ash formation and deposition associated with biomass cofiring with coal were tested in a pilot-scale stoker-fired combustion system at the Energy & Environmental Research Center (EERC).

Experimental

Coal and Biomass Analysis. One representative coal (Cordero Rojo subbituminous) sample and two biomass fuels (wood chips and sunflower hulls) were selected for analysis and combustion testing. The coal and biomass fuels were selected for availability and either current use or the likelihood of future use in commercial applications. All fuels were analyzed for heating value, proximate-ultimate analysis, chlorine, major ash chemistry (i.e., SiO₂, Fe₂O₃, etc.), organically associated elements using chemical fractionation analysis, and mineral content using computer-controlled scanning electron microscopy (CCSEM).

Combustion Testing. The EERC's combustion test facility was modified to simulate a grate-fired system, called the combustion test stoker (CTS). The CTS is an upfired reactor (approximately 32 kg/hr, or 70 lb coal/hr) that contains an existing fouling probe bank to simulate convective surfaces and an electrostatic precipitator (ESP) for particulate control and ash capture. Three single-day combustion tests were completed including a baseline coal test and tests of 40 wt% blends of wood chips and sunflower hulls with the baseline coal. Firing rate was controlled to achieve a minimum furnace exit temperature of 983°C (1800°F) at nominally 20% excess air on a volume basis. Data comparisons included grate ash properties, fly ash properties, and flue gas properties as they pertain to fuel combustion efficiency. Fly ash collected in the ESP was analyzed for carbon content and particle size using a Malvern sizing instrument. Ash deposits were collected from the fouling probe bank and analyzed using scanning electron microscopy and major ash chemistry.

Results and Discussion

Table 1 lists the analysis data for the test fuels. The Cordero Rojo coal is typical of many Powder River Basin (PRB) coals in its

analysis. The sample fired here was drier (20 wt% moisture) than the as-received fuel from the mine (typically 26 wt%). Inorganics were present at the 5.14 wt% level and consisted primarily of silica (31 wt%), alumina (19 wt%), and calcium (25 wt%) on an as-received basis. Sodium was present at about 1 wt%. Chloride content of the coal was measured at 21.3 µg/g.

Table 1. Coal and Biomass Analysis Data

Fuel Description	Cordero Rojo	Wood	Sunflower
	Coal	Chips	Hulls
	As-Fired	As-Fired	As-Fired
Proximate Analysis, wt%			
Moisture	20	5.2	11.4
Volatile Matter	37.61	78.54	72.21
Fixed Carbon	37.25	15.71	13.53
Ash	5.14	0.55	2.85
Ultimate Analysis, wt%			
Hydrogen	5.87	6.28	7
Carbon	53.37	46.46	46.35
Nitrogen	0.67	0.01	1.39
Sulfur	0.23	0.36	0.52
Oxygen	34.72	46.34	41.89
Ash	5.14	0.55	2.85
Heating Value, Btu/lb	9325	7764	7754
Chloride, µg/g	21.3	71.9	
Fuel Size, cm	1.905 × .635	1.27 × 0	.635 × 0
Ash Analysis, wt%			
SiO ₂	31.2	7.52	2.95
Al ₂ O ₃	18.6	1.75	0.83
Fe ₂ O ₃	4.57	8.76	0.71
TiO ₂	1.65	0.41	0.06
P ₂ O ₅	1.24	2.39	14.2
CaO	24.5	33.4	13.6
MgO	5.28	5.48	14
Na ₂ O	0.9	0.88	0.05
K ₂ O	0.42	37	47.2
SO ₃	11.7	2.42	6.38
Select Mineral Phases, wt%			
Quartz	25	2	0
Kaolinite	19	0	0
Mixed Clays	16	12	0
Iron Oxide	1	2	2
Phosphate Mineral	4	0	0
Pyrite	2	2	0
Gypsum	2	35	0
Unclassifiable	11	43	95

The as-fired wood chips were low in moisture (5.2 wt%) and ash (0.55 wt%) and contained a high-volatile-matter component. They were milled to an average size of about 1.3 cm × 0. Because of the low moisture content, the as-fired wood chips had a fairly high heating value. The low ash content was dominated by calcium (33 wt%) and potassium (37 wt%). Chloride content was measured at 71.9 µg/g.

Sunflower hulls were fired as received with no additional preparation. They contained a moderate level of moisture at 11.4 wt% and a fairly low ash content of 2.85 wt%. Heating value and volatile matter were similar to the wood. The inorganic portion of the hulls comprised mainly alkali and alkaline-earth elements: 47 wt% potassium, 14 wt% magnesium, and 14 wt% calcium. Phosphorus

and chloride contents were high relative to the other fuels at 14 wt% and 601 $\mu\text{g/g}$, respectively.

Chemical fractionation indicated that nearly all of the alkali-alkaline-earth elements in the biomass fuels are organically associated, showing extractions of 90% or more from water and ammonium acetate. About 25% of the calcium in the sunflower hulls is extracted in the HCl extraction stage and may be bound as a carbonate. A portion of the calcium (about 40 wt%) and potassium (65 wt%) in the Cordero Rojo coal is tied up with clay materials.

CCSEM analyses indicate quartz (25 wt%), kaolinite (19 wt%), and other mixed clays (16 wt%) as the major mineral phases present in the Cordero Rojo coal. The major mineral phases present in the wood sample were gypsum at 35 wt%, mixed clays at 12 wt%, and high concentrations of unclassifiable minerals (43 wt%), which were either very fine calcium carbonate or “bright” spots of organically bound potassium and calcium. Minor amounts of quartz, iron oxide, mixed clays, and pyrite were present in the wood. The sunflower hulls show little if any discernable mineral matter with the electron microscope except for some iron oxide. Unclassifiable minerals total 95%, which are primarily very fine carbonate or silica structures or “bright” potassium spots in the sunflower organic matrix that are excited by the rastering electron beam and are identified by CCSEM as small particles with a mixed elemental analysis consisting of 50%–95% potassium and an array of other elements. This type of analysis is characteristic of high concentrations of organically bound inorganics with little in discernable mineral particles.

Ash deposition on convective surfaces was minimal for all tests, baseline coal as well as the coal-biomass cofiring tests. Only a few grams of ash were sticking to the ash deposition probe, and the material was mostly calcium and potassium sulfates. The resulting deposition observed would not significantly reduce the capability of a boiler to produce steam. The highest deposit growth rate was observed for the baseline coal. This deposit, however, had the lowest strength of any of the deposits generated. The highest-strength deposit was observed for the 60–40 Cordero Rojo-sunflower hull blend, which also had the lowest growth rate. Analysis of the 60–40 coal-sunflower hull blend deposit showed a potassium-calcium-aluminosilicate bonding matrix essentially “gluing” the deposit together. The high concentration of potassium in the sunflower hulls reacted with the abundant calcium-aluminosilicates derived from the coal, which led to lower-melting-point phases of lower viscosity which tend to increase strength development in ash deposits. Analysis of the 60–40 coal-wood chip blend deposit showed a calcium-iron-aluminosilicate bonding matrix with iron crystallizing out of the melt. The crystallization of the iron can decrease the strength of the melt by creating areas that fracture more readily. The low ash content of the wood chips also contributed to a lower ash deposition rate and strength.

Furnace exit gas temperatures (FEGTs) during the pilot-scale tests ranged from 1021° to 1065°C (1870° to 1948°F). Slightly higher (56°C [100°F]) FEGTs could trigger more severe fouling. Also, the quantity of fly ash generated during these tests was lower than considered typical for stoker-fired applications. Therefore, these observations may have been influenced by some minor grate clinker formation. In summary, the dynamics of the stoker system create cooler burning and flame temperatures, resulting in lower FEGTs, which diminish fouling propensity.

Figure 1 shows that fly ash particle-size distribution decreased when biomass was blended with the coal. This was expected because of the fine size of the fuel minerals in the biomass and the preponderance of organically associated alkali metals and alkaline-earth components. In terms of fly ash generation, the alkalis can be expected to form fine particulates in the form of potassium sulfate,

potassium phosphate, chlorides, and calcium sulfate, among other fine species. The shift to a finer fly ash particle size as a result of biomass cofiring could be problematic for units with small ESPs or, in some cases, old stokers still using multicyclones for particulate control. It is recommended that units lacking adequate ESP surface or using multicyclones consider ESP upgrades or installation of fabric filters for collection of fine particulate to meet emissions standards.

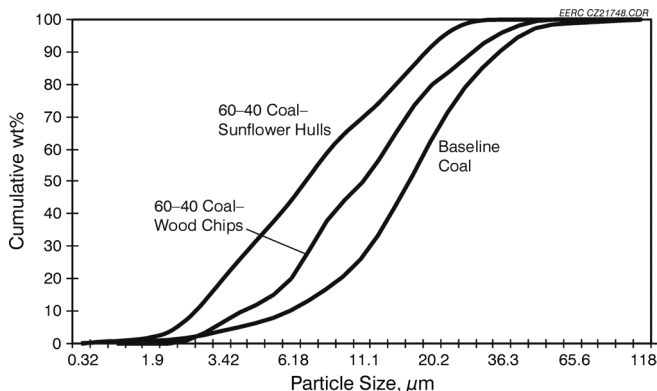


Figure 1. Fly ash-size distribution by Malvern analysis – 60–40 Cordero Rojo-wood chips

Acknowledgment. This work was supported by the United States Department of Energy National Energy Technology Center under Cooperative Agreement No. DE-FC26-00NT41014. The EERC acknowledges NETL Performance Monitor Philip M. Goldberg for his supervision.

References

1. Folkedahl, B.C.; Zygarlicke, C.J. Cofiring Wood Residue and Sunflower Hulls with Coal. In *Proceedings of the 27th International Technical Conference on Coal Utilization & Fuel Systems*; Clearwater, FL, March 4–7, 2002; Vol 1, pp 515–526.
2. Folkedahl, B.C.; Zygarlicke, C.J.; Strege, J. Influence of Biomass Cofiring on PM_{2.5} Ash Produced in a 7-kW Coal Combustion System. Presented at the NETL PM_{2.5} Conference, Pittsburgh, PA, April 9–10, 2002.
3. Folkedahl, B.C.; Zygarlicke, C.J.; Hutton, P.N.; McCollor, D.P. Biomass for Energy – Characterization and Combustion Ash Behavior. In *Proceedings of Power Production in the 21st Century: Impacts of Fuel Quality and Operations*; Harding, N.S.; Baxter, L.L.; Wigley, F.; Frandsen, F., Eds.; Snowbird, UT, Oct 28 – Nov 2, 2001.
4. Sondreal, E.A.; Benson, S.A.; Hurley, J.P.; Mann, M.D.; Pavlish, J.H.; Swanson, M.L.; Weber, G.F.; Zygarlicke, C.J. Review of Advances in Combustion Technology and Biomass Firing. *Fuel Process. Technol.* **2001**, *71* (1–3), 7–38.
5. Zygarlicke, C.J.; McCollor, D.P.; Toman, D.L.; Dahl, J. Ash Interactions During the Cofiring of Biomass with Fossil Fuels. In *Proceedings of the 26th International Technical Conference of Coal Utilization, and Fuel Systems*; Clearwater, FL, March 5–8, 2001; pp 237–248.
6. Frandsen, F.J.; Nielsen, H.P.; Jensen, P.A.; Hansen, L.A.; Livbjerg, H.; Dam-Johansen, K.; Sorensen, H.S.; Larsen, O.H.; Sander, B.; Henriksen, N.; Simonsen, P. Deposition and Corrosion in Straw- and Coal-Straw Co-Fired Utility Boilers. In *Proceedings of the Engineering Foundation Conference on the Impact of Mineral Impurities in Solid Fuel Combustion*; Kona, HI, Nov 2–7, 1997; Wall, T.F.; Baxter, L.L., Eds.; 1997; 14 p.

PREDICTING NO_x EMISSIONS FROM BIOMASS COFIRING

Stephen Niksa^a, Guisu Liu^a, Larry Felix^b, P. Vann Bush^b, and Douglas M. Boylan^c

^aNiksa Energy Associates, 1745 Terrace Drive, Belmont, CA 94002, neasteve@pacbell.net

^bSouthern Research Institute, P. O. Box 55305, Birmingham, AL, 35255-5305

^cSouthern Company Services, Inc., P. O. Box 2641, Birmingham, AL, 35291-8195

Introduction

In theory, biomass cofiring should reduce NO_x emissions simply because most forms of biomass contain less fuel-N than the coals they displace. The yields of volatiles are generally much higher from biomass than from coal, and volatiles contain many compounds that can effectively reduce NO in fuel-rich flame zones. Biomass also decomposes faster than coal, which tends to steepen near-burner temperature profiles and enhance the ignition characteristics. These factors are expected to improve NO_x emissions by more than the displacement of coal-N. But the database from pilot- and full-scale testing exhibits mixed results, including substantial representation for no effect, for less reduction than the displacement of fuel-N, and for enhanced reduction over the displacement of fuel-N.

The premise for our work is that uncontrolled variables are responsible for the ambiguities in the existing database. A testing campaign was staged to characterize the most likely parameters, including the biomass form, coal type, biomass injection configuration, burner staging, and furnace stoichiometry. The database from the testing campaign was then interpreted with simulations based on full chemistry for fuel decomposition, volatiles combustion including fuel-N conversion, soot conversion, and char burnout. Once the model predictions were demonstrated to be accurate, the simulation results were interrogated to determine how the biomass affected NO_x emissions. We find that two factors determine whether biomass cofiring will reduce NO_x emissions: (1) Does the abundance of gaseous volatiles, not soot, from biomass reduce away the NO formed near the burner; and, (2) Is significantly less char-N released into downstream flame zones by the addition of biomass. This paper emphasizes the interpretation of the database with detailed chemical reaction mechanisms. More thorough descriptions of the simulation methodology are available^{1,2}.

Testing Program

All tests were conducted in Southern Research Institute's (SoRI) Combustion Research Facility (CRF). The CRF consists of fuel handling and feeding systems, a vertical refractory lined furnace with a single up-fired burner, a horizontal convective pass, heat exchangers and conventional exhaust cleaning devices. Emissions from this system have been qualified against those from full-scale, tangential-fired furnaces for the operating conditions imposed in this work³. The 8.5 m by 1.07 m (i.d.) cylindrical furnace handles gas velocities from 3 to 6 m/s, and residence times from 1.3 to 2.5 s. The nominal firing rate is 1.0 MW_t, which was fixed for all cases in this work. A single burner generates a core of pulverized fuel and primary air surrounded by weakly swirled secondary air. For all cases in this paper, the biomass was co-milled with the coal and the mixture was directly fed into the burner. Overfire air (OFA) was injected through 4 off-radius ports located 4.6 m down the furnace. All datasets include cases with 0 (unstaged) and 15 % OFA. In the unstaged series, the OFA was combined with secondary air. Air

feedrates were varied to produce exhaust (wet) O₂ levels between 2.5 and 5 %.

Table 1. Fuel Properties

	SD	SG	JR	GL	PR	JW
Proximate, as rec'd						
Moisture	9.5	15.2	19.3	5.8	1.9	0.8
Ash	0.4	29.5	5.4	6.6	15.1	14.6
Volatiles	78.1	47.6	39.6	33.7	33.2	20.0
Carbon	11.9	7.7	35.7	54.0	49.9	64.6
Ultimate, daf wt. %						
C	49.8	56.1	74.9	81.8	83.4	89.5
H	6.1	5.4	4.9	5.0	5.5	4.6
O	43.9	35.7	18.8	10.0	7.5	3.3
N	0.2	2.4	0.9	2.0	1.8	1.7
S	0.0	0.4	0.4	1.1	1.8	0.9
<d _p >, μm	163	173	29	53	48	34

Fuel quality was varied by firing four diverse coals with two forms of biomass. Nominal properties of the six primary fuels appear in Table 1 in order of increasing rank, from left to right. Moisture levels are highest for the low-rank fuels, especially switchgrass (SG) and subbituminous coal (JR). Ash levels are widely variable and especially high for biomass SG and for the hv bituminous (PR) and low volatile bituminous (JW) coals. Whereas it appears that the volatility of sawdust (SD) is much higher than SG's, on a dry-ash-free (daf) basis, their volatiles yields are almost identical. The daf-volatiles contents of the coals fall by more than a factor of two over this suite of samples, which will definitely affect the conversion of coal-N into NO_x. Carbon contents increase and oxygen contents decrease for fuels of progressively higher rank. The pair of biomass samples represents most of the range of elemental compositions seen for diverse forms of biomass. The represented range of coal rank, from subbituminous through lv bituminous, is similarly broad. The hydrogen, nitrogen, and sulfur levels are not rank-dependent. Whereas almost all biomass contains little nitrogen and sulfur, sample SG contained the most nitrogen of any of the fuels, due to its decomposition before firing. The particle size distributions (PSDs) are typical utility grinds for the coals, except for the much finer grind of JR, whereas the biomass grinds are much coarser, as expected.

Computer Simulations

It is not currently possible to incorporate detailed chemical reaction mechanisms into conventional CFD simulations of pulverized fuel (p. f.) flames. Since chemistry in the gas phase, especially volatile-N conversion chemistry, was suspected to play a dominant role in NO_x production during biomass cofiring, Niksa Energy Associates developed a new computational approach for this application based on our "ChemNet™ Post-Processing (CNPP)" method. The CNPP method first generates an equivalent network of idealized reactor elements from a conventional CFD simulation. The reactor network is a computational environment that accommodates realistic chemical reaction mechanisms; indeed, mechanisms with a few thousand elementary chemical reactions can now be simulated on ordinary personal computers, provided that the flow structures are

restricted to the limiting cases of plug flow or perfectly stirred tanks. The network is “equivalent” to the CFD flowfield in so far as it represents the bulk flow patterns in the flow. Such equivalence is actually implemented in terms of the following set of operating conditions: The residence time distributions (RTDs) in the major flow structures are the same in the CFD flowfield and in the section of the reactor network that represents the flow region under consideration. Mean gas temperature histories and the effective ambient temperature for radiant heat transfer are also the same. The entrainment rates of surrounding fluid into a particular flow region are evaluated directly from the CFD simulation. To the extent that the RTD, thermal history, and entrainment rates are similar in the CFD flowfield and reactor network, the chemical kinetics evaluated in the network represents the chemistry in the CFD flowfield. Whereas this paper emphasizes the application to biomass cofiring, separate publications explain the simulation methodology in greater detail^{1,2,4}.

CFD Simulations

CFD simulations of the CRF were performed by Reaction Engineering International (REI) for all tests with PR coal and various biomass. Cases with JR and JW were performed at SoRI, using REI’s Configurable Fireside Simulator (CFS) for the CRF. The CFS imposes a fixed computational grid on the calculations, and is therefore suitable for parametric case studies with the same firing configurations. No CFD were available for cases with the second hv bituminous coal (GL) because these flame structures were expected to be very similar to the PR flames.

The most surprising feature in the CFD simulations is that all fuel particles remained on the furnace axis throughout this furnace. Neither mixing in the near-burner zone nor radial OFA injection disperses the particles off their original trajectories. Near the burner, the primary air stream was significantly expanded by the release of volatiles from the fuel suspension and by thermal expansion. This expansion zone delineates a fuel-rich core from the outer, annular flow of secondary air. Nominal residence times in the core range from 120 to 170 ms. The expansion of the primary flow promotes entrainment of secondary air into the core, because some of the secondary flow penetrates the expansion boundary. In addition, a portion of secondary air is entrained into the core as soon as it passes the edge of its delivery tube in the fuel injector. Together, these entrainment mechanisms almost instantaneously mix about 20 % of the secondary air into the primary flow.

The mixing layer between the core and secondary air streams gradually expands until it contacts the furnace wall midway to the OFA ports. An external recirculation zone (ERZ) forms in the corner bounded by the outer boundary of the secondary air stream, but is too weak to entrain particles or appreciable amounts of air or fuel compounds. As the fuel compounds in the flame core contact the secondary air stream, they mix and burn in an expanding mixing layer. This layer completely surrounds the core near the burner inlet, and fills the entire furnace downstream of the core. The most distinctive feature of the mixing layer is that the temperature profile across the layer in the normal direction passes through a maximum value which is essentially the same around the entire circumference of the core. Maximum gas temperatures approach 1700°C in cases where fuels of the highest heating values were fired without OFA, and 1600°C in cases with 15 % OFA. Residence times in the mixing layer to the OFA location vary from 500 to 600 ms. The four air jets from the OFA ports do not penetrate onto the centerline. They also do not fill the entire flow cross section. Downstream of the OFA ports, the flow relaxes to a plug flow pattern that carries ash and exhaust into an exhaust system. The total residence time from the burner to the furnace exit is approximately 2.5 s.

Equivalent Reactor Network

As seen in Fig. 1, the bulk flow patterns are delineated in the regions assigned by CNPP from the CFD simulation. The baseline PR flame consists of a core, mixing layer, ERZ (which is inconsequential), OFA-region and burnout (BO) region. All other flames have the same regions. The CSTR network from the CNPP analysis of the baseline PR flame also appears in Fig. 1. The networks for all other CRF flames have similar branches and feedstreams but appreciably different quantitative specifications. In the network, the flame core has been subdivided into two regions. The devolatilization zone covers the upstream portion of the core in which volatiles are being released from the fuel suspension and burned with primary air. Since the primary stream is extremely reducing, no residual O₂ leaves the devolatilization zone. The NO_x reduction zone covers the downstream portion of the core in which only the N-species are converted under the influence of water gas shifting, due to the absence of O₂. The CSTR-series for the mixing layer and the OFA zone represent the mixing of secondary and tertiary air streams, respectively. But there are no additional flows into the CSTR-series for the BO zone.

The RTD for this particular core was deconvoluted into one component for 16 CSTRs-in-series and another for plug flow with respective mean residence times of 138 and 193 ms. The plug flow component represents the near-axial fluid motion under the influence of particle drag, and the CSTR-component represents flow with significant radial velocities. The networks for other fuels usually have only one flow channel for the entire core, and the bulk flow pattern is plug flow. The RTD for the mixing layer was matched with a series of 19 CSTRs, and that for the OFA zone was represented by 6 CSTRs-in-series. The BO zone is essentially in plug flow.

Note that entrainment into the various CSTR-series is represented as a series of discrete additions over several reactors in the series. Volatiles are entrained into the series for the first part of the flame core; secondary air is entrained into the series mixing layer; and tertiary air is entrained into the series for the OFA zone. The addition rates of volatiles were specified from the stand-alone devolatilization simulation with the thermal histories of particles from the CFD simulation. The specific addition rates of the air streams were specified from the continuous entrainment profiles evaluated from the CFD simulation.

Reaction Mechanisms

The devolatilization submodel, called FLASHCHAIN[®], determines the complete distribution of volatile compounds from almost any p. f., and also predicts the yield and elemental composition of char⁵. When combined with a swelling factor correlation and a correlation for the initial carbon density in char, it specifies all the necessary char properties for a char oxidation simulation. Hence, the complete distribution of volatiles, including gaseous fuels and soot, and all char properties are completely determined from only the fuel’s proximate and ultimate analyses.

The reaction mechanism for chemistry in the gas phase contains 444 elementary reactions among 66 species, including all relevant radicals and N-species⁶. All rate parameters were assigned independently, so there are also no adjustable parameters in the submodel for gas phase chemistry. The soot chemistry submodel depicts several important effects. As soot burns, it directly competes for the available O₂ and also consumes O-atoms and OH that would otherwise sustain homogeneous chemistry. Soot also promotes recombinations of H-atoms and OH that could also sustain NO homogeneous chemistry⁷. And soot reduces NO directly into N₂.

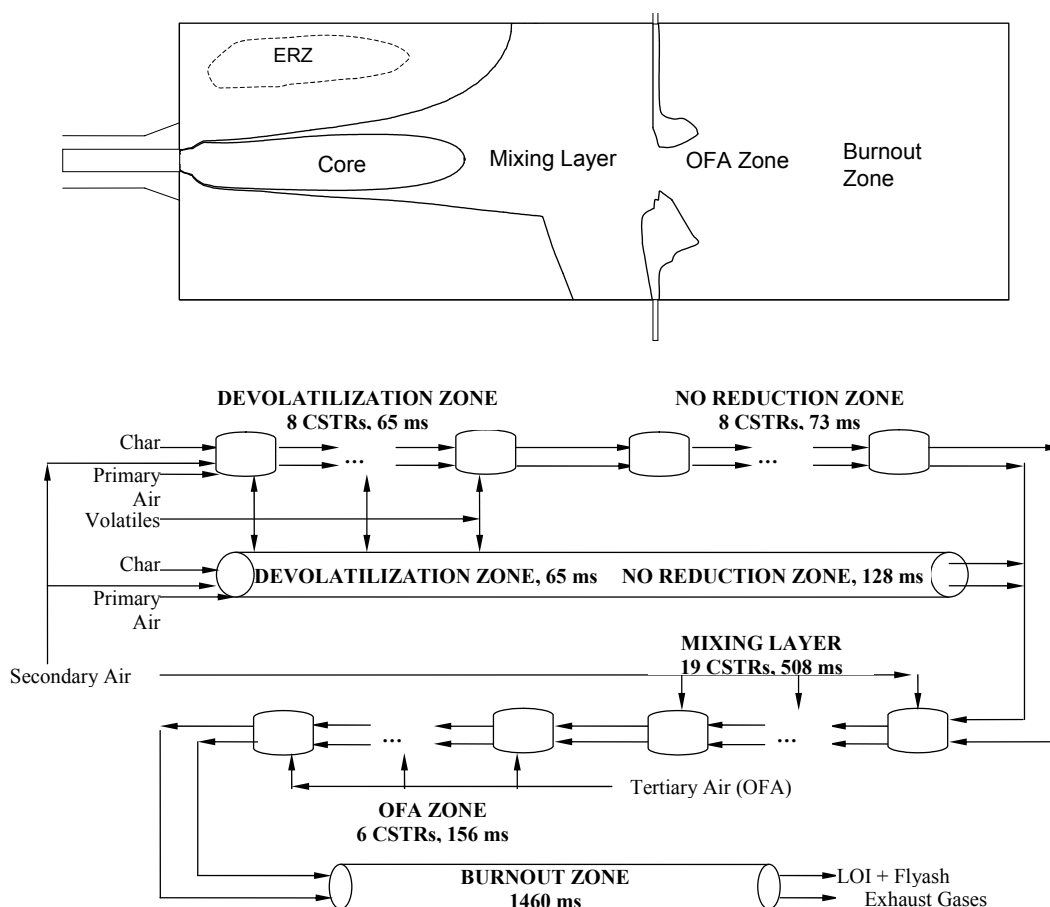


Figure 1. (Top) CNPP regions delineated from the CFD simulation for the baseline PR flame, and (Bottom) equivalent reactor network.

Char burning rates are determined by thermal annealing, ash encapsulation (of low-rank chars), and a transition to chemical kinetic control. The Char Burnout Kinetics (CBK) Model includes all these effects, and depicts the impact of variation in gas temperature, O_2 level, and char particle size within useful quantitative tolerances⁸. However, it is not yet possible to specify the initial char reactivity within useful tolerances from the standard coal properties. We must calibrate this value with LOI predictions or some other suitable index on combustion efficiency. The submodel for char-N conversion is subject to a similar calibration requirement (with NO emissions), compounded by its simplistic mechanistic premise; viz., that a fixed fraction of char-N is converted into NO at the overall burning rate throughout all stages of char oxidation.

To summarize, the initial char reactivity and the fraction of char-N converted to NO can only be specified from calibration procedures, whereby these parameters are adjusted to match the predicted LOI and NO_x emissions to reported values for a single set of operating conditions. Then the same values should be imposed for all other operating conditions. Except for these two parameters, all other model parameters can be assigned from the fuel's proximate and ultimate analyses within useful quantitative tolerances, or directly adopted from literature.

Calibration and Extrapolation Procedures

The fraction of char-N converted to NO during char oxidation was assigned to fit the NO_x emissions from the coal-only baseline flames for each coal sample. These same values were applied in all cofiring simulations. Values for biomass were unnecessary because biomass chars contain no nitrogen.

Only 13 CFD simulations were developed for the CRF under this project, yet almost 300 tests were simulated with detailed reaction mechanisms. All but one of the cases with CFD simulations had 15 % OFA, and were for the coal-only baselines or the high loading of biomass. Extrapolations to operating conditions without CFD were based on perturbations to the flame temperature profiles and air entrainment rates. All these procedures were established for the coal-only baseline flames to describe the reported impact of furnace stoichiometry and staging level on the NO_x emissions. Once established, the same extrapolation procedures were then applied without adjustment to the cofiring cases.

Results

The discussion in this section moves through the mechanistic basis for NO_x reduction via biomass cofiring, beginning with the distinctive devolatilization behavior of the various fuels in the testing program. Then the NO_x predictions are evaluated in comparisons with data, followed by our interpretations for the major trends based on the detailed flame structure of CRF flames.

Table 2. Distributions of Secondary Pyrolysis Products and Char Properties.

	SD	SG	JR	GL	PR	JW
Volatiles, daf wt. %						
Wt. Loss	86.1	86.0	65.2	56.5	59.8	39.7
Soot	4.3	13.4	30.1	33.7	37.9	26.8
CH ₄	7.1	7.4	0.7	0.4	0.5	0.3
C ₂ H ₂	2.2	1.3	1.5	1.0	1.3	2.3
C ₂ H ₄	1.4	1.5	0.0	0.0	0.0	0.0
H ₂	2.1	1.7	3.4	3.6	4.0	3.5
CO	48.4	41.5	12.9	7.2	6.1	1.7
CO ₂	8.2	8.0	6.4	2.2	1.7	1.0
H ₂ O	12.1	7.7	7.6	4.9	4.3	1.8
HCN	0.0	0.0	1.26	2.47	2.24	1.52
NH ₃	0.24	2.90	0.0	0.0	0.0	0.0
H ₂ S	0.0	0.44	0.42	1.17	1.91	0.96
Char Comp., daf wt. %						
C	94.7	97.1	98.9	98.4	98.5	98.2
H	3.4	2.5	0.5	0.5	0.4	0.5
O	1.9	0.4	0.0	0.0	0.0	0.0
N	0.0	0.0	0.4	1.1	1.0	1.26
S	0.0	0.0	0.1	0.1	0.1	0.0
Char ash, wt.%	2.5	75.7	15.9	14.2	30.9	21.8
Char size, μm	97.6	103.6	29.9	59.1	54.1	41.7

Predicted Devolatilization Behavior. Since the heating rate of primary air in the CRF is very fast, the primary devolatilization products are instantaneously converted into secondary volatiles pyrolysis products. The predominant transformation during secondary pyrolysis is the conversion of tar into soot, with simultaneous release of tar-O as CO, tar-H as H₂, and most of the tar-N as HCN. In addition, all aliphatic hydrocarbons are converted into CH₄ and C₂H₂, which can add to the soot phase during the latest stages. The predicted distributions of secondary pyrolysis products are collected in Table 2. Total volatiles yields are the same for both forms of biomass and, at 86 daf wt. %, much higher than the yields from any of the coals. The biomass product distributions are dominated by CO, with substantial amounts of hydrocarbons, especially CH₄, and CO₂ and H₂O. H₂ is another major fuel compound from biomass. But there is surprisingly little soot, considering that tar, the soot precursor, is 25 to 45 % of the daf fuel mass released during primary devolatilization. The reason is the abundance of tar-O, which approaches 40 % of the tar mass. This oxygen converts most of the tar into CO rather than soot during secondary pyrolysis. Essentially all the fuel-N is released as NH₃ during secondary pyrolysis. The abundance of NH₃ with SG, and its higher soot yield and lower CO yield, are the major difference between the two biomass forms.

In contrast, the secondary pyrolysis products from all the coals are dominated by soot which is, by far, the most abundant product. The total hydrocarbon yields are comparable from all coals, but less than a fourth of the hydrocarbon yields from the biomass. Hydrogen yields are also comparable, and double those from biomass. The yields of the oxygenated gases diminish with coals of progressively higher rank, in accord with the trend in the coal-O levels. But even the highest CO yield from JR coal is only about one-quarter the CO yield from the biomass. The only N-species is HCN although, in actuality, a minor amount of NH₃ may have been released from JR coal (but none of the others). The N-species yields are directly proportional to the coal-N levels, as expected.

Char compositions are very similar among all six fuels, except that the most abundant heteroatoms in biomass chars are H and O. versus H and N in the coal-derived chars. The char-N levels are negligible in biomass chars. They are comparable but lower for the coal-derived chars and certainly not negligible. Perhaps the most

Table 3. Evaluation of Predicted NO_x for 3.5 % O₂ with 15 % OFA.

Series	Fuel	NO _x , ppm @ 3 % dry O ₂	
		Pred.	Mes'd
1	PR hv bit	325	328
	PR/10%SD	255	271
	PR/20%SD	236	245
5	PR/15%SG	277	269
	PR/20%SG	258	260
	GL hv bit	372	360
6	GL/10%SD	365	273
	GL/20%SD	318	327
	GL hv bit	368	356
7	GL/10%SG	399	340
	GL/20%SG	349	336
	JR subbit	263	240
12	JR/10%SG	203	185
	JR/20%SG	177	142
	JR/10%SD	221	191
13	JR/20%SD	212	189
	JW lv bit	419	422
	JW/5%SD	416	420
13	JW/10%SD	417	389
	JW/20%SD	436	364
	JW lv bit	429	450
	JW/5%SG	422	455
	JW/10%SG	442	440
	JW/20%SG	404	407

significant variation in char properties is among the char-ash levels. The values for SG and PR are definitely high enough to inhibit char oxidation during the latest stages of burnout, according to the ash inhibition mechanism in CBK. The mean char sizes are disparate for the biomass and coal chars, but more similar than the whole coal values because biomass shrinks and the coals swell during devolatilization, especially the bituminous coals

Evaluation of Predicted NO_x Emissions. The reported impact of fuel quality on NO_x emissions is extremely complex. It depends on which coal is fired, which biomass is cofired, which cofiring level is imposed, and which injection configuration is used. Table 3 presents the measured and predicted NO_x emissions for all cases with co-milled fuel injection and 15 % OFA that had 3.5 % exhaust O₂. Cofiring with 10 % SD always reduced NO_x, except with JR coal (and with GL coal with 0 % OFA). With the same injection, cofiring with 20 % SD reduced NO_x with JR and GL but not with JW. With PR/20 % SD, NO_x was reduced with 15 % OFA (but not with 0 % OFA). Cofiring with 20 % SG was effective on PR and JW, but notwith GL and JR. With 10 % SG, cofiring was effective with JR, but not with GL and JW; PR was not tested at this condition.

As seen in Table 3, the predicted emissions for PR hv bit coal (Ser. 1) are within experimental uncertainty for all biomass cofiring combinations. They correctly depict the more-than-20 % reduction in NO_x with the highest loadings of both biomass forms, and a proportional decrease in NO_x for progressively higher biomass loadings. No discrepancy exceeds 16 ppm. Similarly, the predictions for JR subbit. (Ser. 7) depict the proportional reductions in NO_x with higher biomass loadings, and the greater effectiveness of SD compared to SG. In this series no discrepancy exceeds 35 ppm. Cases with the JW lv bit. coal are within experimental uncertainty for SG co-firing (Ser. 13), which did not reduce NO_x at either of the lower switchgrass loadings. The predicted NO_x reduction with 20 % SG (Ser. 12) was under 10 %, in accord with the measured value. But with SD cofiring on JW coal (Ser. 12), the predictions show no significant NO_x reduction for any SD loading, at

odds with the reported reductions up to 11 % for loadings of 10 and 20 %.

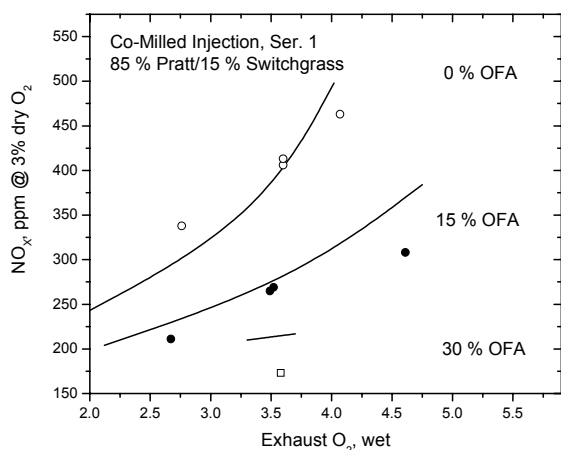


Figure 2. Predicted (Curves) and measured (data points) NO_x emissions for 3 staging levels and a range of exhaust O_2 levels for PR/15 % SG flames.

Predicted NO_x emissions with GL coal (Ser. 5 and 6) are not as accurate as all others, and the reported behavior is more complex. With SD cofiring, the reported extent of NO_x reduction is significantly greater for a 10 % loading than for 20 %. With SG cofiring, the same extent of NO_x reduction was reported for both loadings. But the predicted NO_x emissions are actually higher than the coal-only baselines with both biomass forms. Unfortunately, no CFD simulations were available for any of the GL test cases, so the specifications for PR-coal were applied in all GL-cases. A breakdown in this extrapolation procedure may be responsible for the discrepancies in the predictions, although they may also reflect a flaw in the mechanisms for this particular chemical environment.

The accuracy of the extrapolation procedures for furnace stoichiometry and staging level are apparent in Fig. 2. This set of predictions covers the full ranges of furnace stoichiometry (which determines exhaust O_2 level) and degree of air staging in the test program. The predictions are based on the procedures developed to fit the NO_x emissions for the coal-only baseline tests over the same domain of conditions, starting with only a single CFD simulation for 3.5 % O_2 and 15 % OFA. The same procedures were then applied without modification to the biomass cofiring cases, such as the 15 % SG on PR in Fig. 2. The predictions are within experimental uncertainty except, perhaps, for the highest O_2 level with 15 % OFA. Notwithstanding, it is evident that these extrapolations did not introduce intolerable uncertainties into the predictions, and CNPP can be successfully applied with many fewer CFD simulations than test conditions.

Discussion

The predicted structure of the flame core for the PR/20%SD flame appears in Fig. 3. In contrast to SG, SD has almost no fuel-N. This cofired flame still generates 25% less NO_x than the PR-only baseline flame, which is slightly more than the reduction expected for the removal of fuel-N alone. The time scale in Fig. 3 depicts the core as well as the first quarter of the mixing layer. For this particular test, devolatilization is completed within 80 ms, and the flow leaves the core at 118 ms. The total residence time in the mixing layer is 476 ms, but only the first 150 ms are shown in Fig. 3.

The S. R. value for the gas phase falls sharply while volatiles are released into the flow, making it more reducing. It then relaxes to an ultimate value 0.864, which is significantly more reducing than both the PR-only baseline and the PR/20%SG flame. Although SD and SG have identical volatiles yields, the gas phase in the SD-core becomes more reducing because more CO and less soot are produced by the primary volatiles from SD.

Initially, the CO concentration surges during the ignition period, then increases more gradually during the oxidation of char and soot. Its ultimate value and the persistence of H_2 reflect water gas shifting once all O_2 has been consumed. The maximum CO concentration is double that in the PR/20%SG flame. The H_2 mass fraction persists at roughly 1000-2000 ppmw across the entire core. Moreover, hydrocarbons, especially C_2H_2 (not shown), persist at 1000 ppmw or more across the entire devolatilization zone. This is the only flame core with an appreciable amount of hydrocarbons in the presence of NO, although their concentration is still much lower than those of CO and H_2 .

As for the other flames, almost half the char burns out in the core, but hardly any soot burns out in this particular core. The more reducing character of the gas phase in this core imparts several distinctive features to the N-species conversion chemistry. The N-speciation is dominated by HCN and NO, as for the PR-only baseline flame. The NH_3 released by the SD is rapidly converted to HCN and NO within 40 ms. But NO does not accumulate at the expense of HCN, as in both of the other flame cores. Instead, the HCN concentration surges while NO accumulates. Some prompt N-fixation mechanisms involving N_2 in air must be responsible because the total maximum amount of fixed-N species is double the maximum value in the PR/20%SG flame, and the SG-cofired flame has significantly more volatile-N. NO reduction begins at 75 ms but by the exit of the core, there is still 1390 ppmw HCN and 465 ppmw NO, which are both much higher than in either of the other flames. Early in the mixing layer, NO reduction accelerates while the HCN concentration plummets. The NH_3 concentration reaches 92 ppm before vanishing with the HCN concentration. The ultimate NO concentration after both other fixed-N species have been eliminated is only 143 ppmw, which is 25 ppm lower than the analogous level in the PR/20%SG flame. Even though there was a higher concentration of fixed-N species in the core, the greater reducing potential yielded a lower NO concentration in the mixing layer, after chemistry in the gas phase was exhausted. Since the extents of char burnout at this point are comparable for the PR/20%SG and PR/20%SD flames, the 20 ppmw reduction for the PR/20%SD flame persists in the exhaust emissions.

A surge in the extent of soot burnout coincides with the entrainment of secondary air. Due to the high maximum temperatures in the mixing layer, the extent of soot oxidation eventually overtakes the extent of char oxidation at 220 ms. The soot burns out in the mixing layer, whereas char is carried over into the OFA and BO regions.

The structures of the coal-only and the biomass cofired flames in the CRF are qualitatively similar: All exhibit a very rapid surge in the NO level immediately after injection, due to the ignition of volatiles under the very lean conditions associated with the primary streams during the initial stages of devolatilization. But as more volatiles are released, the gas phase becomes progressively more reducing, which enables the early NO to be reduced into HCN and NH_3 . The extent of reduction is determined by the S. R. value among the gaseous species only and the residence time available before the core fluid is exposed to secondary air in the mixing layer. All fixed-N species are rapidly converted into NO and N_2 at the beginning of the mixing layer, which then sustains the oxidation of soot and char.

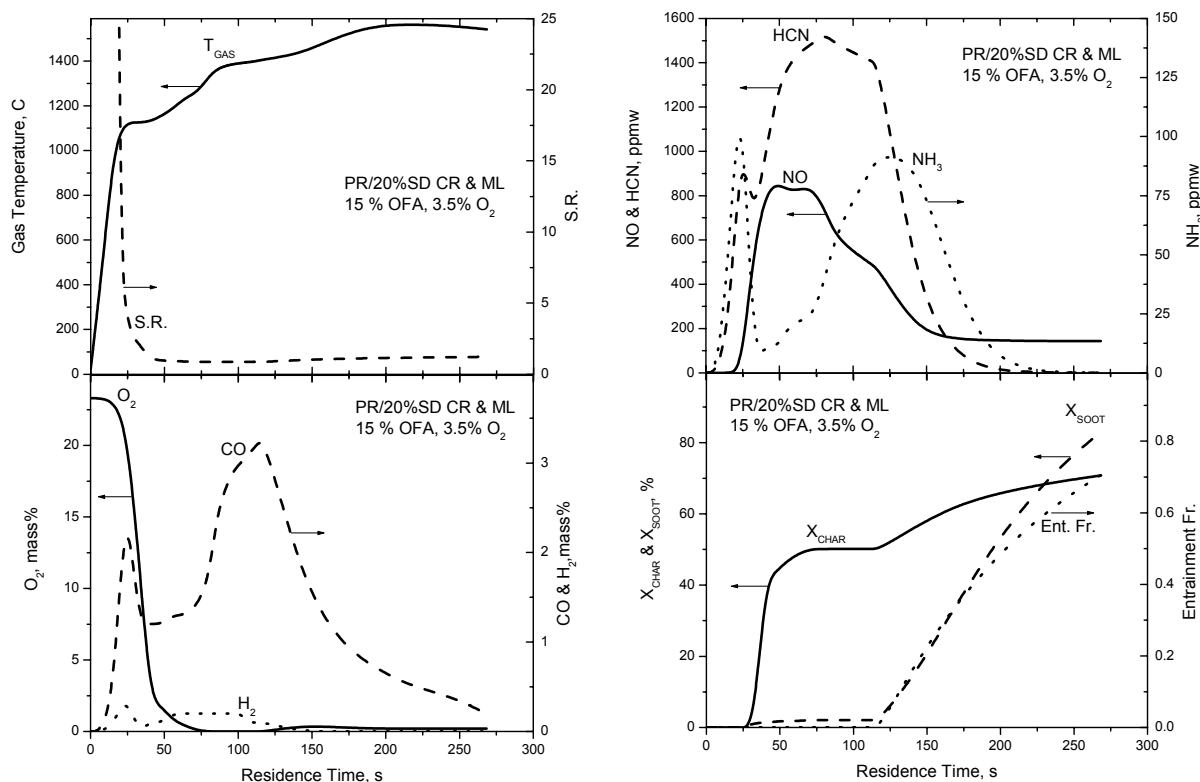


Figure 3. Structure of the core of the PR/20%SD flame showing, in counterclockwise order from the upper left, the operating conditions, major species, char and soot burnout, and N-species.

From this point onward, chemistry in the gas phase is inconsequential, and the conversion of some of the char-N into NO supplements the NO_x inventory.

Two factors are primarily responsible for the significant NO_x reduction observed for CRF flames with biomass cofiring. First, there is more volatile matter from biomass and it contains a much smaller contribution from soot. Consequently, the near-burner S. R. values for the gas phase are significantly richer than in coal-only flames. Under richer conditions, near-burner NO will be reduced away and a greater proportion of the fixed-N species will be converted into N₂. CRF flames provide sufficient residence times in the flame cores for NO reduction and fixed-N conversion to N₂. Second, a significantly lower percentage of the total fuel-N will remain in the char beyond the near-burner zone, where its partial conversion to NO is inevitable. If the biomass contains nitrogen, it releases all of it in the near-burner zone. If the biomass contains no nitrogen, then the inventory of char-N beyond the flame core is reduced in proportion to the biomass loading. In either case, there is less char-N beyond the point where NO can be reduced by chemistry in the gas phase.

The first factor is especially sensitive to fuel quality. Indeed, even the NO_x emissions from the four coal-only flames are ordered according to the volatiles yields and contributions from soot. While the volatiles yields decrease and the soot contributions increase for coals JR, PR, GL, and JW (cf. Table 2), the baseline NO_x emissions in the staged flames increased from 240 to 338 to 358 to 436 ppm (cf. Table 3). Biomass cofiring mitigated these differences by enhancing volatiles yields and by reducing the soot contributions. The net effect was significant NO_x reduction for the cofired flames,

even when the biomass supplements the inventory of fuel-N. The extent of reduction was directly proportional to the biomass loading with both forms of biomass on JR and PR coals. But it was only proportional to the SG loading in flames cofired with JW coal; cofiring JW with sawdust was ineffective at all but the highest loadings. Cofiring GL coal reduced NO_x, but the magnitude was disproportionate at 10% loadings with both biomass forms.

Acknowledgement. This work was partially sponsored by an award (DE-FC26-00NT40895) under the Biomass Cofiring Opportunities Program administered by the National Energy Technology Laboratory.

References

- (1) Niksa, S.; and Liu G.-S., *Fuel*, **2002**, 81(18),2371-85.
- (2) Niksa, S.; and Liu, G.-S., "Advanced CFD Post-Processing for P. F. Flame Structure and Emissions," 28th Int. Technical Conf. on Coal Utilization and Fuel Systems, **2003**, Coal Technology Assoc., Clearwater, FL, March.
- (3) Monroe, L. S. et al., 1995, EPRI/EPA 1995 Joint Symp. On Stationary Combustion NO_x Control, Book 3, EPRI, Palo Alto, CA.
- (4) Niksa, S.; and Liu, G.-S. *Proc. Comb. Inst.*, **2002**, 29, to appear.
- (5) Niksa, S. *Combust. Flame*, **1995**, 100, 384-394.
- (6) Glarborg, P.; Alzueta, M. U.; Dam-Johansen, K.; and Miller, J. A. *Combust. Flame*, **1998**, 115, 1-27.
- (7) Pedersen, L. S.; Glarborg, P.; et al. *Combust. Sci. Technol.*, **1998**, 132, 251-314.
- (8) Hurt, R. H.; Sun J.-K.; and Lunden, M. *Combust. Flame*, **1997**, 113(1/2), 181.

STUDY ON THE MECHANISM OF NO_x FORMATION FOR CO-COMBUSTION OF PULVERIZED COAL AND BIOMASS

Xiaoqian Ma¹, Shiyun Su¹, Zengli Zhao², Xiaobing Zhang^{1,3}, Yong Chen²

¹College of Electric Engineering, South China University of Technology, Guangzhou, 510640, China

²Guangzhou Institute of Energy Conversion, Chinese Academy of Sciences, Guangzhou, 510070, China

³City College and Graduate School of The City University of New York, New York, 10031, U.S.

Introduction

A problem of much concern about coal combustion is the contaminations of NO_x, among which ~ 95% is NO.¹ People have been studying the co-combustion of coal powder and biomass for the following reasons.²⁻⁴ 1. Since the heat value of biomass (pulverized wood and rice hull are studied in the paper) is usually lower than coal, substituting coal with a proper amount of biomass can decrease the burning temperature, especially at the rear part of the furnace where most NO_x is produced. 2. The coke produced in biomass combustion can reduce NO so that less NO is released. 3. The co-combustion of coal powder and biomass helps utilize the non-recyclable source. In the paper, using the burning temperature data of coal powder in one dimension furnace, we numerically calculate the amounts of produced NO when the coal powder is and is not mixed with biomass. Also calculated are the amounts of reduced NO by HCN and by coke which are produced in co-combustion when the effects of the biomass on temperature is and is not taken into consideration. We shall find out capability of different biomasses to reduce NO_x.

Computing Model

The simplifications which the calculation is based on are as follows: 1. The axial length of the one dimension furnace meets the requirement of large space jet; 2. The heat loss by radiation, the body force and the effects on flow by the chemical reactions are negligible so that the combustion can be approximated as adiabatic; 3. The properties do not change with temperature or composition. Shown in Table 1 are the known parameters of the jet.^{5,6} in which b_0 is the half width of the jet exit, a the jet flow constant, u_0 initial velocity of the jet flow, Y_0 the initial partial mass concentration, and Y_∞ the ambient partial mass concentration.

Table 1. Known parameters of the jet

b_0	a	u_0	Y_0			Y_∞		
			O ₂	N ₂	HCN	O ₂	N ₂	H C N
7	0.105	29.4	0.188	0.7	6.04×10^{-5}	0.21	0.78	0

Listed below are the formulae used to compute the co-combustion reaction rate of pulverized coal and biomass.

$$R_{HCN \rightarrow NO} = 10^{11} \rho_g Y_{HCN} (Y_{O_2})^c \exp\left(-\frac{33700}{T_g}\right) \quad (1)$$

$$R_{NO-N_2} = 3 \times 10^{12} \rho_g Y_{HCN} Y_{NO} \exp\left(-\frac{33700}{T_g}\right) \quad (2)$$

$$R_{N_2-NO} = 3 \times 10^{14} \rho_g^{1.5} Y_{N_2} Y_{O_2}^{0.5} e^{\frac{-65300}{T_g}} \frac{M_{NO}}{M_{N_2} M_{O_2}^{0.5}} \quad (3)$$

$$R_{NO-N_2} = 4.24 \times 10^4 \frac{A_E m_{char}}{VOL} P Y_{NO_{SUP}} e^{\frac{1.465 \times 10^8}{RT_g}} M_{NO} \quad (4)$$

in which $R_{\alpha-\beta}$ is the rate at which α is converted to β in kg/m³/s, ρ_g the mixed gas density in kg/m³, Y_α the partial mass concentration of composition α , c the reaction coefficient whose value is set to be 0.4 here, T_g the gas temperature in K, VOL the coke volume in m³, M_α the molar mass of α in g/mol, A_E the particle surface area of coke, which is set at 0.7 m²/g, m_{char} the coke mass rate in g/s, P the total pressure in atm, $Y_{NO_{SUP}}$ the partial NO mass concentration on coke surface, and R the gas constant in kJ/kg/K.

Results

The results we obtain are shown in the following figures. A variable B is defined to indicate the ratio of the mass flow rates of biomass and coal powder. The parameters used to run the calculation can be obtained by writing to the correspondence author Ma, Xiaoqian at epqxma@scut.edu.cn.

(1) Temperature distribution without the effects of biomass

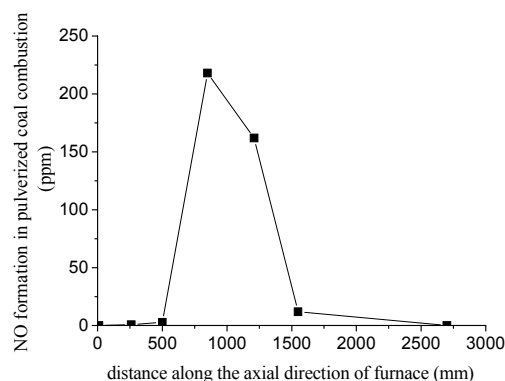


Figure 1. NO formation distribution in pulverized coal combustion without the effects of biomass on temperature.

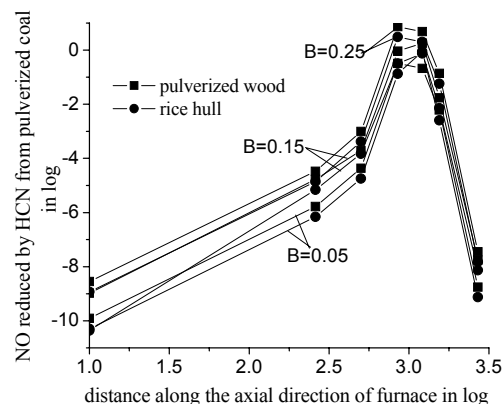


Figure 2. Distribution of reduced NO by HCN from pulverized coal in co-combustion without the effects of biomass on temperature.

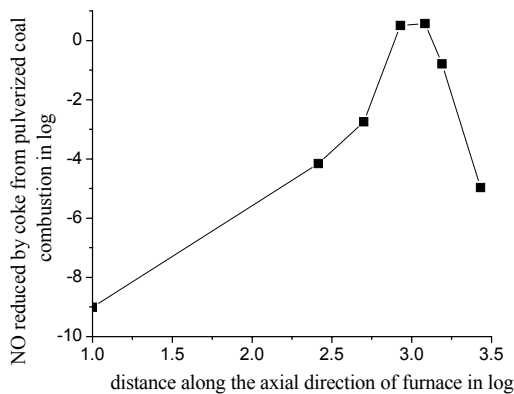


Figure 3. Distribution of reduced NO by coke from pulverized coal in co-combustion without the effects of biomass on temperature.

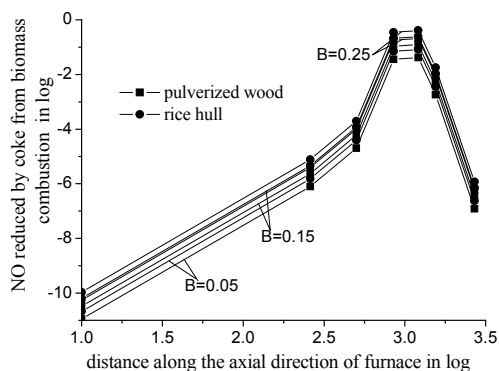


Figure 4. Distribution of reduced NO by coke from biomass in co-combustion without the effects of biomass on temperature.

(2) Temperature distribution with the effects of biomass combustion by means of energy balance
Equations (1)-(4) can be used to analyze the reduction capability.

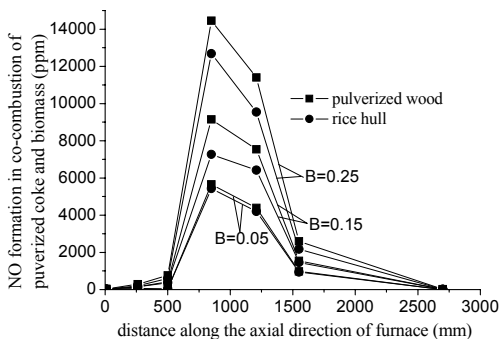


Figure 5. NO formation distribution in co-combustion with the effects of biomass on temperature.

Discussion and Conclusions

Temperature is a factor of importance on NO formation. Due to the limited space available here, we would like to skip this point and emphasize on the NO reduction by HCN and coke produced in the combustion. Figures 2-4 show that in co-combustion when the effects of biomass on temperature are neglected, the reduced NO by HCN, and by the coke in the pulverized coal combustion and in the co-combustion of coal powder and biomass, are in the same order, all of

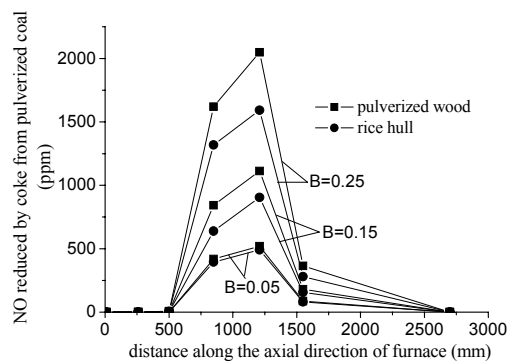


Figure 6. Distribution of reduced NO by coke from pulverized coal in co-combustion with the effects of biomass on temperature

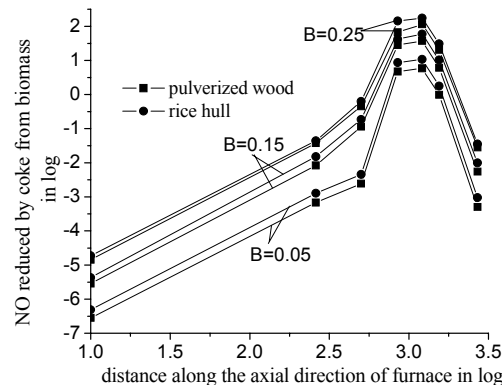


Figure 7. Distribution of reduced NO by coke from biomass in co-combustion with the effects of biomass on temperature

which are vanishingly little compared with the total amount of the produced NO. With the effects of biomass on temperature, the coke from pulverized coal elevates the amount of reduced NO, as indicated in Figure 6. The elevation is enhanced with increasing B, and more when pulverized wood is co-combusted than when rice hull is. Shown in Figure 7 is the distribution of reduced NO by coke from biomass at different B in co-combustion. The increment in amount of reduced NO with growing B increases by orders of magnitude, and the increment rate is far larger than that of the NO formation (see Figure 5), and that of the NO reduction by coke from pulverized coal (see Figure 6).

References

1. Zhao, J. In *Emission Contamination and Noise of Thermal Power Equipments* [C]; Science Press: Beijing, 1995.
2. Purvis, M. R. I.; Tadulan, E. I.; and Tariq, A. S. *Int. J. Energy Res.*, 2000, **24**: 917-933.
3. Skreiberg, O.; Glarborg, P.; Jensen, A.; and Dam-Johnansen, K. *Fuel*, 1997, **76**(7): 671-682.
4. Brink, A.; Bostrom, S.; Kilpinen, P.; and Hupa, M. *IFRF Combust. J.*, 2001. NO. 200107.
5. Han, C.; Xu, M.; Zhou, H.; and Qiu, J. In *Coal Combustion* [C], Science Press: Beijing, 2001.
6. Li, C.; and Tan, L. *Fuel*, 2000, **79**(15): 1899-1906.